



**HAL**  
open science

## Early Pleistocene hominin teeth from Gongwangling of Lantian, Central China

Lei Pan, Clément Zanolli, María Martín-Torres, José María Bermúdez de Castro, Laura Martín-Francés, Song Xing, Wu Liu

► **To cite this version:**

Lei Pan, Clément Zanolli, María Martín-Torres, José María Bermúdez de Castro, Laura Martín-Francés, et al.. Early Pleistocene hominin teeth from Gongwangling of Lantian, Central China. *Journal of Human Evolution*, 2022, 10.1016/j.jhevol.2022.103212 . hal-03864545

**HAL Id: hal-03864545**

**<https://hal.science/hal-03864545>**

Submitted on 21 Nov 2022

**HAL** is a multi-disciplinary open access archive for the deposit and dissemination of scientific research documents, whether they are published or not. The documents may come from teaching and research institutions in France or abroad, or from public or private research centers.

L'archive ouverte pluridisciplinaire **HAL**, est destinée au dépôt et à la diffusion de documents scientifiques de niveau recherche, publiés ou non, émanant des établissements d'enseignement et de recherche français ou étrangers, des laboratoires publics ou privés.

## Early Pleistocene hominin teeth from Gongwangling of Lantian, Central China

Lei Pan, Clément Zanolli, María Martínón-Torres, José María Bermúdez de Castro, Laura Martín-Francés, Song Xing, Wu Liu

### Abstract

The fossil hominin individual from Gongwangling of Lantian, Central China, represents one of the earliest members attributed to *Homo erectus* in East Asia. Recent paleomagnetic analyses have yielded an age of 1.63 Ma for the Gongwangling hominin. The fossils from this site are critical to characterize the morphological features of early hominins in East Asia and to understand their relationships with other earlier and later members of the genus *Homo*. However, most morphological details of the Gongwangling cranium were obliterated due to postmortem erosion and deformation. Here we used high-resolution microcomputed tomography and three-dimensional virtual imaging techniques to extract the teeth and reconstruct the worn/damaged areas, describe the external morphology, measure crown diameters, record nonmetric traits of the crown and root, and investigate the shape of the enamel-dentine junction using geometric morphometrics. We compared the data obtained from the six teeth of the Gongwangling hominin with African early *Homo*, African and Georgian *Homo erectus* s.l., Asian *Homo erectus*, *Homo antecessor*, pre-Neanderthals, Neanderthals, and modern humans. Our results show that the Gongwangling specimens display affinities with other specimens attributed to *H. erectus* s.l. The highly divergent and noncoalesced three-root system in the Gongwangling specimens is comparable to that in the Early Pleistocene members of *H. erectus* s.l., and differs from Middle Pleistocene representatives of the species. The enamel-dentine junction shape of the Gongwangling molars prefigures the Asian *H. erectus* pattern later found in East Asian Middle Pleistocene *H. erectus*. The morphological comparisons between East Asian Early Pleistocene (e.g., Gongwangling, Meipu, and Quyuan River Mouth) and Middle Pleistocene *H. erectus* (e.g., Zhoukoudian, Hexian, and Yiyuan) suggest a potential temporal trend within this species in East Asia.

### Keywords

Lantian

Dental morphology

*Homo erectus*

East Asia

Diffeomorphic surface matching

### 1. Introduction

The Gongwangling paleoanthropological fossil site is situated north of the Qinling Mountains, on the southern part of the Loess Plateau, in northern China (Woo, 1966a). Discovered in 1964 in an Early Pleistocene deposit, the Gongwangling human cranial remains of a single individual labeled PA105 include the frontal and parietal bones, the right temporal bone, portions of the nasal bones, a portion of the maxilla with five teeth, and an isolated maxillary molar (Woo, 1964, 1966a). Faunal and palynological studies made at the site suggested an age of ca. 700 ka for the fossil-bearing layers (Aigner and Laughlin, 1973). Paleomagnetic polarity of the sediments in relation to the stratigraphic position of the hominin remains suggested chronological ages of 800–750 ka (Ma et al., 1978), 1.0 Ma (Cheng et al., 1978), or 1.15 Ma (An and Ho, 1989). A recent re-examination of the deposit has revealed a major stratigraphic hiatus above the

fossil-bearing layer, suggesting an estimated age of 1.63 Ma (Zhu et al., 2015) that is comparable to the age of 1.66 Ma obtained for the oldest lithic assemblages at Majuangou, in the Nihewan Basin, North China (Zhu et al., 2004).  $^{26}\text{Al}/^{10}\text{Be}$  burial dating of the top of a gravel bed around 7 m below the Gongwangling fossil layer yielded a burial age of 1.82 Ma (Tu et al., 2017). Based on these findings, the Gongwangling hominin PA105 appears to represent some of the earliest evidence of human occupation in this continent and thus constitutes a key specimen to better understand the earliest hominin settlements in East Asia.

Upon discovery, PA105 was attributed to *Homo erectus* and has been described and discussed in detail (Woo, 1965, 1966a, b). With its massive supraorbital ridges, low frontal squama, low cranial height, and estimated small cranial capacity (780 cm<sup>3</sup>), the Gongwangling hominin appears to have a more primitive morphology than *H. erectus* from Zhoukoudian and Trinil (Woo, 1966a). However, most of the morphological details of the cranium were obliterated due to postmortem erosion and distortion (Shang et al., 2008), limiting the accuracy of the morphological investigations and the estimation of endocranium volume. The teeth, by contrast, are well preserved, although occlusal wear and some cracks limit interpretations of the external morphology.

Following the discovery of the Gongwangling specimen, more dental remains of Early and Middle Pleistocene *H. erectus* s.l., as well as other Early Pleistocene hominins, were reported and investigated in Eurasia (Grine and Franzen, 1994; Bermúdez de Castro et al., 1999; Martínón-Torres et al., 2008). *H. erectus* s.l. was defined as a single polytypic, widely dispersed species that displays a similar morphological pattern among African and Asian members and also exhibits variation that might be related to geographical separation and/or temporal span (Delson et al., 2000; Antón, 2003). In addition, increased morphological diversity has been recognized in the East-Southeast Asian *H. erectus* hypodigm (Liu et al., 2017; Zanolli et al., 2018a; Pan et al., 2020). Given the increased morphological diversity in Asia, comparisons between the Gongwangling hominin and other Early Pleistocene to Middle Pleistocene *H. erectus* s.l. are needed to further understand its affinities with other members of the species.

High-resolution microcomputed tomography ( $\mu\text{CT}$ ) and three-dimensional (3D) virtual imaging techniques enable the exploration of the internal structural organization of human fossil remains, the virtual reconstruction of damaged specimens, and the quantitative comparison of anatomical structures (e.g., Vialet et al., 2010; Smith et al., 2012; Skinner et al., 2015). For example, using  $\mu\text{CT}$  imaging, it was possible to virtually reconstruct the bony labyrinth of the Gongwangling specimen and to identify similarities with the *Australopithecus africanus* specimens Sts 5 and Sts 19, as well as with the *H. erectus* material from Hexian (Wu and Zhang, 2016). While the cranial bones are heavily distorted and fragmented, the teeth still preserve their original shape despite occlusal wear and some breakage. Previous studies have shown that the quantitative analyses of the inner dental structure can provide information on taxonomy, phylogeny, function/biomechanics, and adaptive changes (e.g., Olejniczak et al., 2008; Skinner et al., 2008a, b; Benazzi et al., 2011; Macchiarelli et al., 2013; Xing et al., 2014, 2015, 2021; Pan et al., 2016, 2017; Zanolli et al., 2018a, 2019; Pan and Zanolli, 2019). Thus, we carried out a detailed description and analysis of the external and internal morphology of the six teeth of the Gongwangling specimen. We compared the dental structure of PA105 with African early *Homo*, African and Georgian *H. erectus* s.l., Asian *H. erectus*, *Homo antecessor*, pre-Neanderthals, Neanderthals, and modern humans. We aim to assess whether the teeth show structural features that are similar to Early Pleistocene *H. erectus* s.l. groups or if they show derived traits as in East Asian Middle Pleistocene *H. erectus*. We also assess if the chronological variation observed in

the Chinese *H. erectus* hypodigm is compatible with the presence of a single lineage or if a larger paleodiversity can be detected.

## 2. Materials and methods

### 2.1. Study samples

The six teeth from the Gongwangling PA105 specimen (i.e., five in situ in the maxilla and an isolated molar) were examined in the present study (Fig. 1). These include the roots of the upper left lateral incisor (LI<sup>2</sup>), the upper right third premolar (RP<sup>3</sup>), and the upper right first molar (RM<sup>1</sup>), as well as three complete teeth representing the right (in situ) and left (isolated) upper second molars (RM<sup>2</sup> and LM<sup>2</sup>) and the upper right third molar (RM<sup>3</sup>). The Gongwangling fossil is stored at the Institute of Vertebrate Paleontology and Paleoanthropology (IVPP), Chinese Academy of Sciences, China.

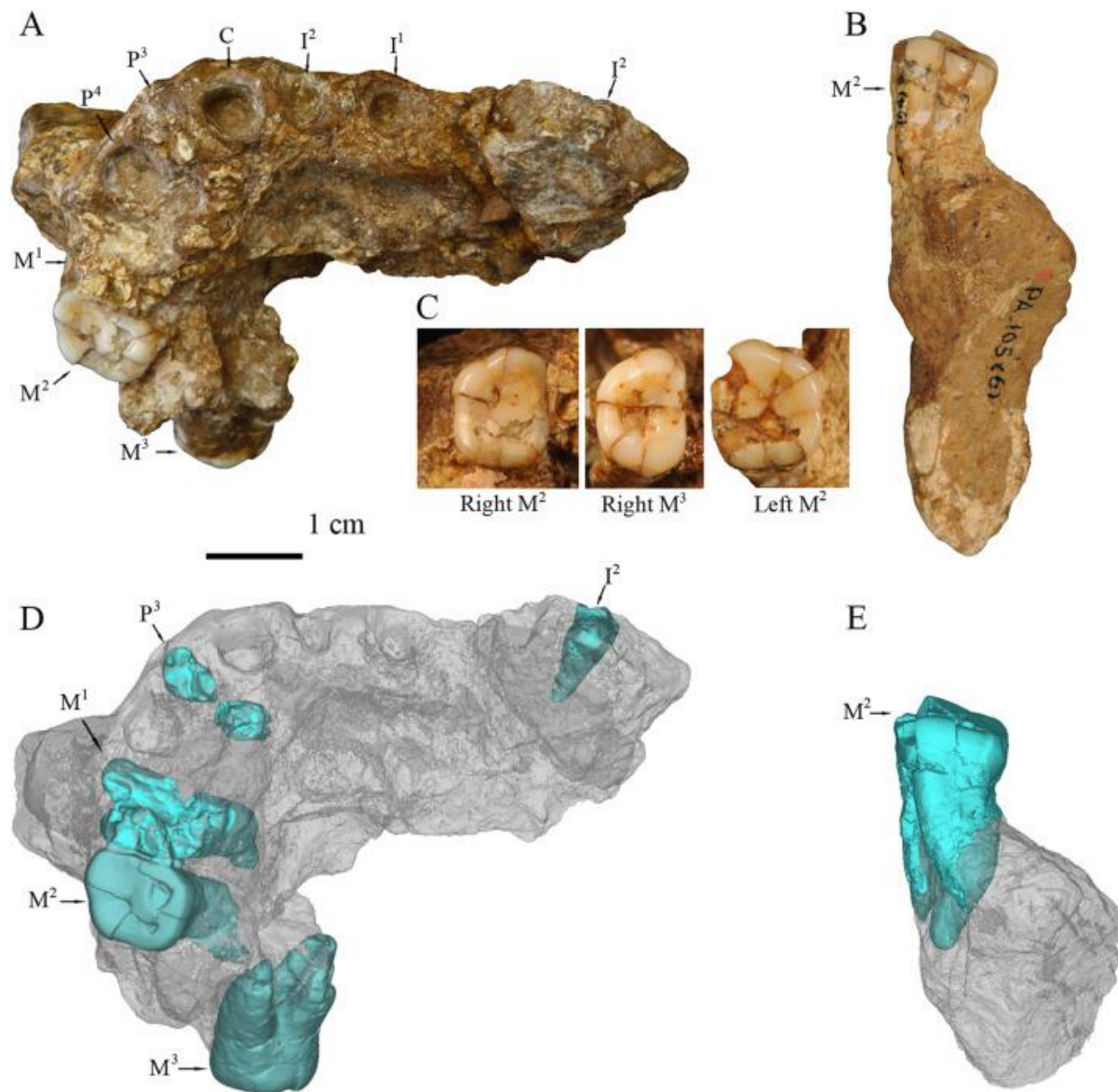


Figure 1. Photographs of the original fossils of the Gongwangling maxilla (A: occlusal view, B: lingual view, C: occlusal view) and virtual reconstructions (D: occlusal view, E: lingual view) of the teeth with the maxilla appearing in semitransparency.

The Gongwangling teeth were compared with those of various *Homo* species/groups (Table 1; Supplementary Online Material (SOM) Table S1). African *H. erectus* s.l. specimens are curated at the Kenya National Museum (Kenya), and Sangiran Early Pleistocene *H. erectus* s.l. teeth are stored at the Senckenberg Research Institute (Germany). SK 847, used in the diffeomorphic surface matching analyses, is stored in the collections of Ditsong Museum of Natural History (South Africa). East Asian mid-Middle Pleistocene *H. erectus* specimens are curated at the IVPP (China), Shandong Museum (China), and Uppsala University (Sweden). To explore evolutionary trends in dental morphology, we compared the PA 105 specimen to earlier fossil hominins and modern humans. Fossil hominins included Early Pleistocene *Homo* (original fossils, Kenya National Museum, Kenya; casts, University of the Witwatersrand, South Africa), later members of the genus *Homo* including European Early Pleistocene *H. antecessor* from Atapuerca TD6 and pre-Neanderthals from Atapuerca Sima de los Huesos (SH), housed at the Spanish National Research Center for Human Evolution (CENIEH, Spain) and Museo of Burgos (Spain), and Neanderthals from Krapina housed at the Croatian National Museum (Croatia). The comparative modern human material is curated at the Institute of Archeology and Cultural Relics of Hubei Province (China), in the Pigorini Museum (Italy), and in the Pretoria Bone Collection of the University of Pretoria (South Africa). The list of comparative specimens and their inclusion in the various analyses described below are detailed in SOM Table S1.

Table 1. Description of the comparative taxa/groups included in the various analyses of this study.

<b>Taxon</b>	<b>Chronology</b>	<b>Geography</b>	<b>Sites</b>	<b><i>n</i></b>
Early <i>Homo</i>	Early Pleistocene	Eastern and southern Africa	Koobi Fora, Olduvai, Sterkfontein	14
<i>Homo erectus</i> s.l.	Early Pleistocene	Eastern Africa, west Asia	Koobi Fora, Nariokotome, Swartkrans, Dmanisi	10
<i>Homo erectus</i>	Early–Middle Pleistocene	Southeast Asia and East Asia	Sangiran, Hexian, Zhoukoudian	47
<i>Homo antecessor</i>	Early Pleistocene	Europe	Atapuerca-TD6	4
pre-Neanderthals	Middle Pleistocene	Europe	Atapuerca-SH	54
Neanderthals	Late Pleistocene	Europe	Krapina, La Chaise-de-Vouthon	29
Modern humans	Holocene	Worldwide	Europe, Asia, and Africa	240

Abbreviations: SH = Sima de los Huesos.

## 2.2. Morphological description and crown size

Outer enamel surface morphology was described following the terminology in the studies by Weidenreich (1937) and Scott and Turner (1997).

Hypocone size of the RM<sup>2</sup>, LM<sup>2</sup>, and RM<sup>3</sup> was scored following the Arizona State University Dental Anthropology System (ASUDAS; Turner et al., 1991). We used the scoring of hypocone size to explore evolutionary trends.

Mesiodistal (MD) and buccolingual (BL) crown diameters for the RM<sup>2</sup>, LM<sup>2</sup>, and RM<sup>3</sup> were measured by one of the authors (S.X.) with a standard sliding caliper and recorded to the nearest 0.1 mm. The interproximal wear facet was taken into account and restored following the profile of the crown contour. The MD and BL diameters were used to estimate and compare crown size between the Gongwangling teeth and other hominin samples.

### 2.3. Microcomputed tomography and surface reconstruction

The maxillary fragment bearing five teeth (PA105-4) was scanned using a 225-kV  $\mu$ CT scanner housed at the IVPP, with the following parameters: 150 kV voltage, 140 mA current, and 52.7  $\mu$ m isotropic voxel size. The isolated LM<sup>2</sup> of PA105-6 was scanned under settings of 140 kV voltage, 120 mA current, and 21.9  $\mu$ m isotropic voxel size. A semiautomatic threshold-based segmentation was conducted on the enamel-dentine junction (EDJ) of RM<sup>2</sup> and RM<sup>3</sup> in Avizo v. 8.0 (FEI Visualization Sciences Group, Houston), following the half-maximum height method, by taking repeated measurements on different slices of the virtual stack (Fajardo et al., 2002; Spoor et al., 2003). The slightly distorted fragments of the RM<sup>2</sup> and RM<sup>3</sup> were restored by displacing the tooth fragments along the breakages and realigning them in correct anatomical position, and the worn dentine horn tips of the RM<sup>2</sup> were reconstructed in Avizo. We did not attempt virtual reconstruction of the LM<sup>2</sup> EDJ due to its more damaged state. The moderately worn dentine horn apices of the RM<sup>2</sup> were reconstructed following a geometric method validated in previous studies (Zanolli et al., 2018b, 2019, 2022). Specifically, the virtual slices of each tooth were resampled to be parallel to the cervical plane. This plane was then translated into each dentine horn extremity, and two sections perpendicular to the cervical plane—corresponding, respectively, to the widest mesiodistal and buccolingual diameters of the last section of the dentine horn and intersecting its center—were used to reconstruct the height and orientation of each apex (for a visual illustration of the various steps to reconstruct the dentine horns, please see Zanolli et al., 2018b: Fig. S1). Interpolations then were performed for rendering the 3D shape of the tips. Virtual surfaces were generated using ‘unconstrained smoothing’ in Avizo. The EDJ surfaces of RM<sup>2</sup> and RM<sup>3</sup> reconstructed and restored in Avizo were used in the diffeomorphic surface matching. The outer surfaces of LI<sup>2</sup>, RP<sup>3</sup>, RM<sup>1</sup>, RM<sup>2</sup>, LM<sup>2</sup>, and RM<sup>3</sup>, EDJ surfaces of RM<sup>2</sup> and RM<sup>3</sup>, and the pulp cavities of LI<sup>2</sup>, RP<sup>3</sup>, RM<sup>1</sup>, RM<sup>2</sup>, and RM<sup>3</sup> were virtually rendered in Mimics v. 17.0 (Materialise, Leuven) for virtual presentation and comparisons.

### 2.4. Enamel thickness of the right upper molar

We measured two-dimensional (2D) and 3D enamel thickness proportions for the Gongwangling RM<sup>3</sup>. We did not measure enamel thickness on the M<sup>2</sup>s due to their more damaged and worn states. Two-dimensional enamel thickness was included to allow for comparisons with other specimens for which only 2D data are available.

To measure 2D enamel thickness, a 2D sectional plane of the crown was defined following Olejniczak (2006). The dentine horn tips of the paracone, protocone, and metacone were used to set a horizontal plane, and then a mesial sectional plane was defined as perpendicular to this horizontal plane and simultaneously cutting through the dentine horn tips of the paracone and protocone (for an illustration of the method, refer to the study by Benazzi et al., 2014: Fig. 2). The areas of the enamel cap (*c*, mm<sup>2</sup>) and dentine and pulp (*b*, mm<sup>2</sup>) and the length of the EDJ (*e*, mm) were measured in ImageJ v. 1.45s (Schneider et al., 2012). Two-dimensional

average enamel thickness (AET) was calculated as  $c/e$ , and relative enamel thickness (RET) was measured as  $(AET/\sqrt{b}) \times 100$ . Because the enamel is slightly worn, we estimated the missing enamel following the method introduced in the study by Saunders et al. (2007; SOM Fig. S2) and we provided estimates of corrected enamel area, and the corresponding 2D AET and 2D RET estimates that were then used in the comparative analyses (we also provided the uncorrected values for the enamel area and enamel thickness indices).

We measured 3D enamel thickness following Benazzi et al. (2014). The crown was separated from the root along the cervical line in Avizo, and the cervical line was interpolated by a surface (for an illustration of the method, refer to the study by Benazzi et al., 2014: Fig. 1). Enamel volume ( $V_e$ ,  $\text{mm}^3$ ), surface area of the EDJ (SEDJ,  $\text{mm}^2$ ), and coronal dentine volume including the volume of the coronal pulp ( $V_{cdp}$ ,  $\text{mm}^3$ ) were measured. Three-dimensional average enamel thickness (3D AET) was calculated as  $V_e/\text{SEDJ}$ , and 3D relative enamel thickness (3D RET) as  $[100 \times 3D \text{ AET}/(V_{cdp}^{1/3})]$  (Kono, 2004; Olejniczak et al., 2008; Benazzi et al., 2014; Zanolli et al., 2018a). All 3D measurements were carried out in Avizo.

## 2.5. Diffeomorphic surface matching of the enamel-dentine junction

A mesh-based, diffeomorphic surface matching (DSM) approach (Beaudet et al., 2016; Zanolli et al., 2018a, 2022; Braga et al., 2019; Pan et al., 2019, 2020) was employed to quantify and compare the EDJ shape of the  $\text{RM}^2$  and  $\text{RM}^3$  (the more damaged states of  $\text{LM}^2$  precluded DSM analysis of this tooth). This landmark-free method superimposes different objects according to their local and global geometric characteristics and establishes correspondences between them (Braga et al., 2019, Dumoncel et al., 2014, Durrleman et al., 2012a, Durrleman et al., 2012b, Durrleman et al., 2014). The surface deformations between different objects are mathematically modeled as diffeomorphisms (Beaudet et al., 2016, Braga et al., 2019, Durrleman et al., 2012a, Durrleman et al., 2014). This method computes a mean shape of the study sample and records the deformations from the mean shape to each object (Pan et al., 2020). In addition, the control points that are situated at the most variable locations of the shape and the momenta parameterizing the surface deformations from the mean shape to each object of the sample are generated (Beaudet et al., 2016, Durrleman et al., 2012a, Durrleman et al., 2012b, Durrleman et al., 2014).

For each dental category, the EDJ surfaces were manually aligned and then superimposed with the reference surface using the rigid and uniform scale option of the ‘Align Surfaces’ module in Avizo v. 8.0 (FEI Visualization Sciences Group, Houston; Pan et al., 2020). The deformations between EDJ surfaces were then calculated using Deformetrica v. 4.3 ([www.deformetrica.org](http://www.deformetrica.org); Bône et al., 2018).

The files of control points and momenta generated by Deformetrica v. 4.3 ([www.deformetrica.org](http://www.deformetrica.org); Bône et al., 2018) were imported into R v. 4.1.0 (R Core Team, 2021) with the package ‘RToolsForDeformetrica’ v. 0.1 (Dumoncel, 2021). Using the package ‘ade4’ v. 1.7–17 (Dray and Dufour, 2007) for R v. 4.1.0 (R Core Team, 2021), weighted between-group principal component analyses (bgPCA; Mitteroecker and Bookstein, 2011) were performed based on the deformation-based shape residuals, and canonical variate analyses (CVAs) were conducted based on the first 10 and eight principal components (for  $\text{M}^2$ s and  $\text{M}^3$ s analyses, respectively), representing ca. 80% of the total variance and corresponding to the highest predictive accuracy scores. Both bgPCA and CVA were conducted based on the same a priori groups (*H. erectus* s.l., pre-Neanderthals + Neanderthals, and modern humans), and the Gongwangling teeth were projected a posteriori in the analyses. We conducted both bgPCA and CVA analyses as they provide complementary information. The bgPCA predictions and posterior probabilities of the

Gongwangling RM<sup>2</sup> and RM<sup>3</sup> compared with *H. erectus* s.l., pre-Neanderthals and Neanderthals, and modern humans were provided. Cross-validated (cv)-bgPCA and CVA of the EDJ shape of *H. erectus* s.l., pre-Neanderthals and Neanderthals, and modern humans were also performed to check that group separation in the weighted bgPCA is not spurious (Cardini and Polly, 2020). Classification frequencies of the cv-bgPCA and CVA, as well as a bivariate plot of the cv-bgPC2 vs. cv-bgPC1, show that the comparative groups are well differentiated (SOM Table S2; SOM Fig. S1). The extreme conformations along the first two bgPC axes (bgPC1 and bgPC2) were generated using Deformetrica, and then the magnitude of displacements between global mean shape to each extreme conformation was rendered as colormaps from dark blue (lowest values) to red (highest values) onto the EDJ surfaces, using the package ‘gtools’ v. 3.9.2 (Warnes et al., 2020) and ‘freesurferformats’ v. 0.1.15 (Schäfer, 2021) in R v. 4.1.0 (R Core Team, 2021).

### **3. Results**

#### **3.1. Descriptive morphology of the Gongwangling teeth**

Upper left lateral incisor The Gongwangling I<sup>2</sup> crown is missing, while most of the root is preserved except for a small part of the cervix and of the apex (Fig. 2). There is a shallow longitudinal groove on the mesial surface of the root. From the cervical line to the apex, the root gradually narrows and is lingually tilted. A similar shape can be observed on the single root canal (Fig. 3).

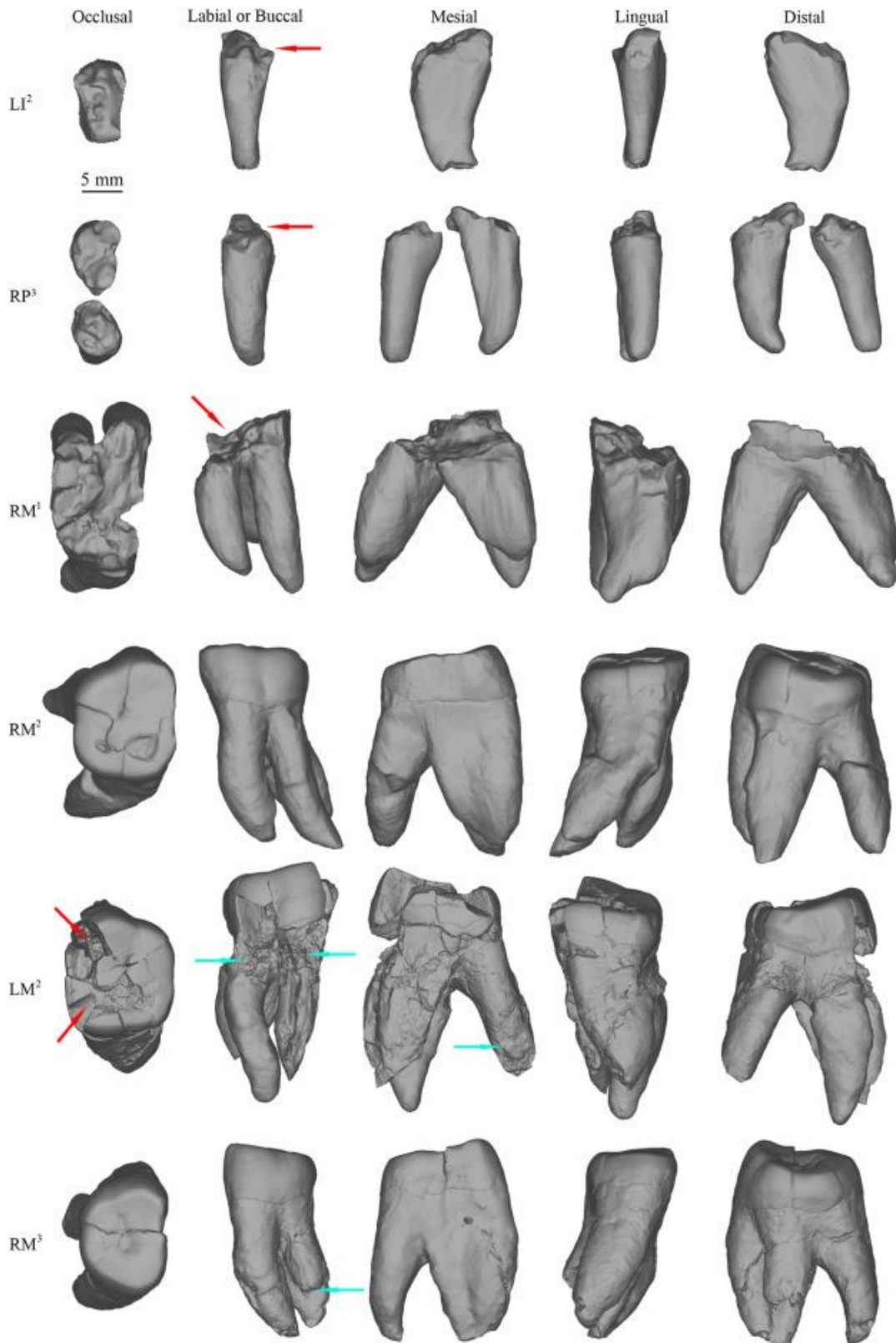


Figure 2. From left to right, occlusal, labial or buccal, mesial, lingual, and distal views of the virtual renderings of the external morphology of the six Gongwangling teeth. Red and cyan arrows point to the broken crowns and roots, respectively.

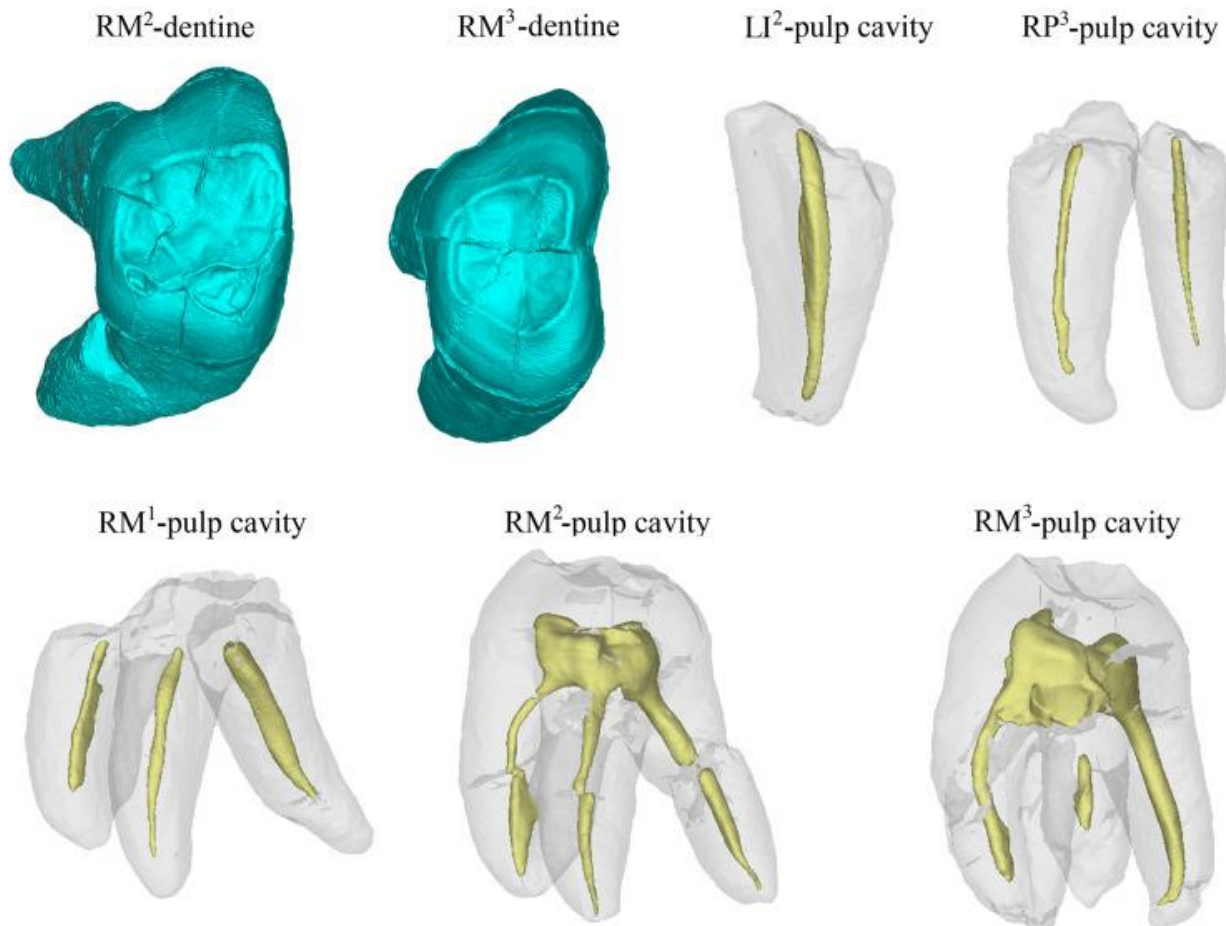


Figure 3. Occlusal view of the enamel-dentine junction surface (RM<sup>2</sup> and RM<sup>3</sup>) and distobuccal view of the pulp cavities of the LI<sup>2</sup>, RP<sup>3</sup>, RM<sup>1</sup>, RM<sup>2</sup>, and RM<sup>3</sup>, reconstructed based on  $\mu$ CT scanning. For the pulp cavities, the cementum and dentine are shown in semitransparency. R = right, L = left. The broken reconstruction of canal branches of the RM<sup>2</sup> and RM<sup>3</sup> is due to their unclear border from the dentine because of breakage and/or deposit filling.

Upper right third premolar The Gongwangling P<sup>3</sup> is represented only by the two completely separated roots and root canals that are highly divergent (Figure 2, Figure 3). There is a longitudinal groove on the mesial aspect of the buccal root. The buccal root tapers gradually from the cervical line to the apex and is deflected lingually toward the apex. The lingual root is column-like and slightly tapers from cervical line to the apex.

Upper right first molar The crown is completely missing except for a small area along the cervical line. Most of the roots are preserved (Fig. 2). The root system is composed of three large, completely separated, and highly divergent branches (Figure 2, Figure 3). The apex of the lingual root is abruptly shrunk.

Upper right second molar This tooth is complete (Figure 1, Figure 2), with an occlusal wear of grade 3 according to Molnar's system (1971). Dentine is exposed in the protocone and hypocone, forming small but unconnected patches. In the occlusal view, the crown outline is trapezoid-like, the mesial aspect being buccolingually wider than the distal aspect. Despite the moderate occlusal wear, the four main cusps—paracone, protocone, metacone, and hypocone—can still be

discerned. The size of the metacone is slightly smaller than that of the paracone, and the hypocone is medium-sized (ASUDAS grade 3.5). No metaconule or cusp 5 is visible at the EDJ (Fig. 3). The crista obliqua is continuous at both the outer enamel surface and EDJ. Two mesial marginal accessory ridges are visible at the EDJ (Fig. 3). The three roots are robust, completely separated, and highly divergent (Figure 2, Figure 3).

Upper left second molar There are some enamel and dentine cracks on the crown, especially on the mesial aspect (Figure 1, Figure 2). Due to this damage, it is impossible to precisely define the degree of occlusal wear, even if the small wear patch on the hypocone is of similar size as in the right M<sup>2</sup>. The crown outline is similar to a trapezoid with a wider mesial portion. The metacone is slightly smaller than the paracone, and the hypocone is medium-sized (ASUDAS grade 3.5). The root system is comprised of three large, completely separated, and highly divergent radicals (Fig. 2).

Upper right third molar This tooth is complete but shows a crack in the mesiodistal direction along the middle of the crown (Figure 1, Figure 2). Although occlusal wear eliminated most of the crown morphology, the four main cusps could be distinguished and there is no exposed dentine, which corresponds to a wear grade 2 (Molnar, 1971). The hypocone is small (ASUDAS grade 3). The crown outline is close to a symmetrical trapezoid with both the metacone and hypocone reduced in size. On the EDJ, no cusp 5 is visible, and the crista obliqua is completely interrupted (Fig. 3). The essential crests of the paracone, protocone, and metacone are low and short. At least two mesial marginal accessory ridges could be observed. Three completely separated and highly divergent radicals and root canals constitute the root system (Figure 2, Figure 3).

### 3.2. Comparative morphology

Upper lateral incisor The curved buccal profile of the Gongwangling I<sup>2</sup> root resemble that of Dmanisi D2677, Zhoukoudian ZKD 7, pre-Neanderthals, and Neanderthals (Weidenreich, 1937; Martínón-Torres et al., 2008; SOM Table S3). Although the lingually deflected root apex could also be observed in Dmanisi D2677, the Gongwangling I<sup>2</sup> expressed it in a more pronounced degree with a curved lingual profile. The taxonomic variability of this feature remains to be addressed.

Upper third premolar A double-separated root is typical in the P<sup>3</sup>s of *H. erectus*, such as in Zhoukoudian ZKD 19 and Yiyuan Sh.y. 003 from East Asia (Xing et al., 2016, 2018; Pan and Zanolli, 2019) and Sangiran 17, 7–27, and 7–58 (Kaifu, 2006; SOM Table S3). In some specimens, the two roots are not completely separated, such as in Zhoukoudian ZKD77 and ZKD78 (Weidenreich, 1937) and Dmanisi D3672 (Martínón-Torres et al., 2008). Comparatively, there are three roots in Hexian PA832 (Xing et al., 2014) and Sangiran 7–35. A three-rooted structure was observed in four out of 8 African early *Homo* specimens (Hughes and Tobias, 1977; Tobias, 1991; Wood, 1991). The individual H1 (ATD6-7) of *H. antecessor* has a P<sup>3</sup> with double roots that are connected by a dentine sheet (Bermúdez de Castro et al., 1999). Pre-Neanderthals (64.3%) from Sima de los Huesos exhibit two roots, and there are cases of a single root (Martínón-Torres et al., 2012). Two-root P<sup>3</sup>s are also common in Krapina Neanderthals (CT data; NESPOS database, 2021), but they are not as divergent as those of *H. erectus* s.l. In modern humans observed in the present study, more than half of the P<sup>3</sup>s have a two-root system, including those with bifid apices. However, when viewed laterally, the root breadth tends to reduce from the cervical line to the apex. The root morphologies of comparative specimens were mainly observed from the outer surface. Micro-CT scans and 3D virtual reconstruction will help further elucidate the complete structure of root system. Beyond the number of radicals, it is noteworthy that the column-like shape of the Gongwangling roots is also found in Hexian PA832

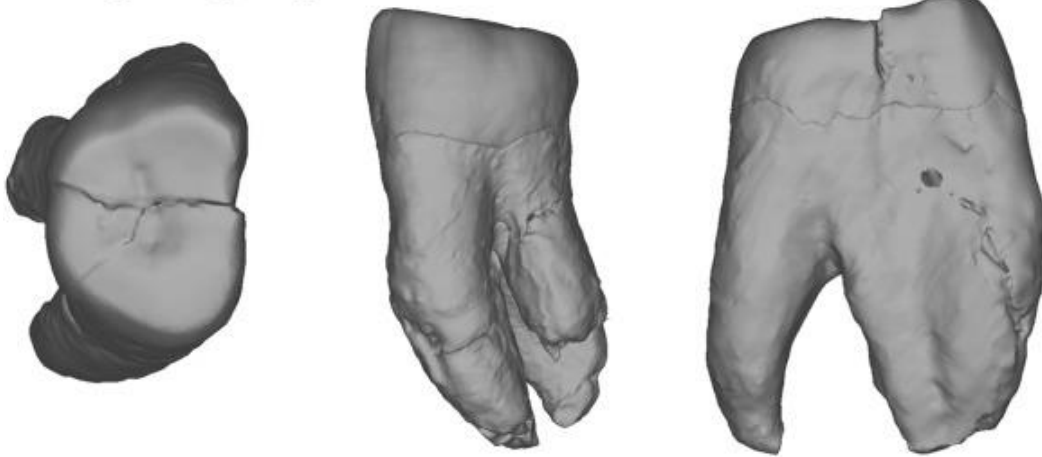
(Xing et al., 2014), but is different from that of Dmanisi where radicals run parallel and narrow toward the apical end.

Upper first molar Three highly divergent roots observed in the Gongwanling M<sup>1</sup> also exist in Sangiran 17 (Kaifu, 2006), Dmanisi D2710 (Martín-Torres et al., 2008), and Zhoukoudian ZKD33 (Weidenreich, 1937; SOM Table S3). The degree of divergence is reduced in European Early and Middle Pleistocene hominins (Bermúdez de Castro et al., 1999; Martín-Torres et al., 2012), Krapina Neanderthals (CT data; NESPOS database, 2021), and modern humans observed in the present study. In aspects of shape, Gongwanling roots are comparatively longer and thicker than those at Dmanisi (Martín-Torres et al., 2008) and Meipu (Xing et al., 2021). In addition, narrowing of the lingual radical of the Gongwanling M<sup>1</sup> is not apparent until the apical end, distinct from the gradually tapering radical in Dmanisi D2710 (Martín-Torres et al., 2008).

Upper second molar The M<sup>2</sup> hypocone in Sangiran, Dmanisi, Zhoukoudian, Hexian, and Yiyuan is generally medium-sized or large (Martín-Torres et al., 2008; Xing et al., 2014, 2016; SOM Table S3). With a medium-sized hypocone, the Gongwanling M<sup>2</sup> falls well within this variation. The M<sup>2</sup> of African early *Homo* is also characterized by a medium-sized or large hypocone, despite an even larger hypocone in KNM-ER 1813. European Early Pleistocene hominins from Atapuerca TD6 have a large hypocone (Bermúdez de Castro et al., 1999; Martín-Torres et al., 2019). Pre-Neanderthals, Neanderthals, and modern humans generally vary from grade 0 to 5 in hypocone size (Martín-Torres et al., 2012). A three-rooted radicular complex with marked divergence, as observed in Gongwanling specimen, can be found in African early *Homo* (OH 16, StW 53) and Sangiran 17 (Kaifu, 2006). In pre-Neanderthals, Neanderthals, and modern humans, M<sup>2</sup>s have a less divergent root system than that of Gongwanling and, in some cases, the radicals coalesce (Martín-Torres et al., 2012). The EDJ surface of the Gongwanling M<sup>2</sup> is simple without the profuse crenulations observed in East Asian Middle Pleistocene specimens such as in Hexian PA833 and PA837 (Xing et al., 2014) and Sh.y. 008 (Xing et al., 2016).

Upper third molar The small hypocone (grade 3) of Gongwanling M<sup>3</sup> is compatible with the range of variation expressed by the Zhoukoudian hypodigm (grade 1 to 4; Weidenreich, 1937; SOM Table S3). The hypocone of Sangiran, Dmanisi, and African *H. erectus* s.l. (KNM-ER 807) generally varies from grades 3 to 4 (Martín-Torres et al., 2008). African early *Homo* M<sup>3</sup>s generally have a hypocone of grade 3.5 to 4, but there is also a small hypocone in OH 16. The hypocone in pre-Neanderthals, Neanderthals, and modern humans varies from grade 0 to 4 (Martín-Torres et al., 2012). Three completely separated and highly divergent roots are rarely seen in East Asian Middle Pleistocene *H. erectus*. In ZKD46, 49, 112, and PMU M3550 (Weidenreich, 1937; Zanolli et al., 2018a), the three roots tend to coalesce and the radicals are more parallel to each other (Fig. 4). Three divergent roots could be found in Sangiran 17 (Kaifu, 2006). OH 15 of African early *Homo* has a completely separated and divergent three-root structure. The radical systems in pre-Neanderthals, Neanderthals, and modern humans tend to coalesce, and they are not as divergent as those in Gongwanling (Martín-Torres et al., 2012). It is noteworthy that Xujiayao of late Middle Pleistocene (Xing et al., 2015) also have three highly divergent roots.

Gongwangling PA105-4



Zhoukoudian PMU M3550



Zhoukoudian ZKD 46

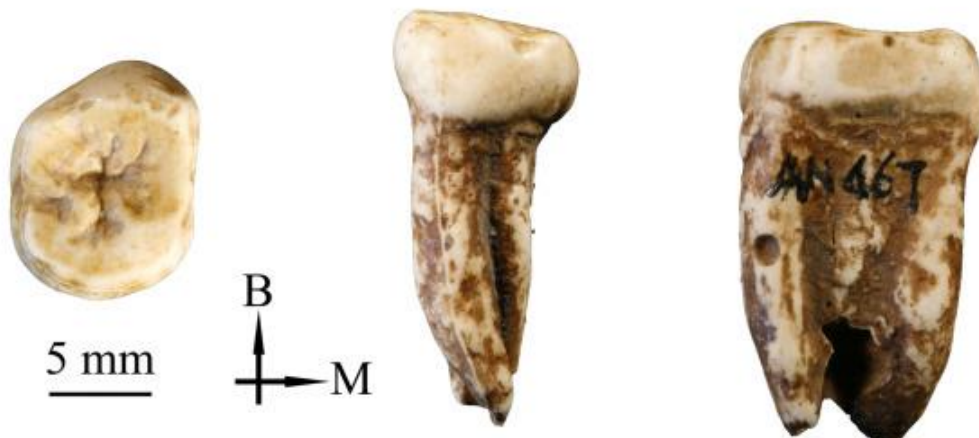


Figure 4. Comparisons of the Gongwangling RM<sup>3</sup> with Zhoukoudian PMU M3550 (virtual reconstruction based on  $\mu$ CT data) and Zhoukoudian ZKD46 (cast) to show the outer enamel morphologies and root structure. Each tooth was presented from left to right in occlusal, buccal, and mesial views. B = buccal; M = mesial; R = right.

### 3.3. Mesiodistal and buccolingual diameters of the M<sup>2</sup>s and RM<sup>3</sup>

The MD diameters of the Gongwangling RM<sup>2</sup> (PA 105-4) and LM<sup>2</sup> (PA 105-6) fall within the ranges of variation for East Asian mid-Middle Pleistocene *H. erectus* but are smaller than African Early Pleistocene early *Homo* and African Early Pleistocene *H. erectus* s.l., West Asian Early Pleistocene *H. erectus* s.l., and most Southeast Asian Early Pleistocene *H. erectus* (Table 2; Fig. 5). The BL diameters of these M<sup>2</sup>s fall within the ranges of variation of all comparative groups (even if they fall in the superior range of West Asian Early Pleistocene *H. erectus* s.l.), except for the African Early Pleistocene *Homo* group that shows larger diameters (Table 2; Fig. 5). The bivariate plot of BL vs. MD diameters shows that the Gongwangling RM<sup>2</sup> and LM<sup>2</sup> fall within the range of variation for East Asian mid-Middle Pleistocene *H. erectus* and pre-Neanderthals (Fig. 5).

Table 2. Crown dimensions of the fossil hominin teeth from Gongwangling and the comparative specimens.

Sample	M <sup>2</sup>							M <sup>3</sup>						
	n	MD (mm)			BL (mm)			n	MD (mm)			BL (mm)		
		Single value/mean	SD	Range	Single value/mean	SD	Range		Single value/mean	SD	Range	Single value/mean	SD	Range
Gongwangling (PA105-4) <sup>a,b</sup>	1	10.8	–	–	13.0	–	–	1	9.6	–	–	13.3	–	–
Gongwangling (PA105-6) <sup>a,b</sup>	1	11.3	–	–	13.3	—	—	–	–	–	–	–	–	–
African Early Pleistocene early <i>Homo</i>	10	12.9	1.1	11.4–14.6	14.7	1.4	13.5–17.6	10	13.0	1.1	11.2–14.4	15.0	1.4	13.2–16.7
African Early Pleistocene <i>Homo erectus</i> s.l.	5	12.5	0.7	11.7–13.3	13.1	1.0	11.7–14.2	1	11.4	–	—	12.9	–	—
West Asian Early Pleistocene <i>Homo erectus</i> s.l.	3	12.2	0.4	11.8–12.5	12.8	0.7	12.1–13.4	1	9.8	–	—	11.9	–	–
Southeast Asian Early Pleistocene <i>Homo erectus</i>	6	12.3	1.1	11.2–13.5	13.5	1.2	12.5–15.5	7	10.3	1.0	9.4–12.4	12.9	1.3	11.5–15.3
East Asian mid-Middle Pleistocene <i>Homo erectus</i>	6	11.2	0.9	10.2–12.5	13.7	1.1	12.3–15.5	8	9.7	0.6	8.7–10.4	11.7	0.8	10.4–12.5

Sample	M <sup>2</sup>						M <sup>3</sup>							
	n	MD (mm)			BL (mm)			n	MD (mm)			BL (mm)		
		Single value/mean	SD	Range	Single value/mean	SD	Range		Single value/mean	SD	Range	Single value/mean	SD	Range
European Early Pleistocene <i>Homo antecessor</i>	1	12.1	—	—	13.7	—	—	—	—	—	—	—	—	—
Pre-Neanderthals	30	9.9	1.0	8.0–11.6	12.1	0.7	11.0–13.8	28	8.6	0.6	7.4–9.6	11.4	0.9	10.0–13.0

Abbreviations: MD = mesiodistal diameter; BL = buccolingual diameter. The crown sizes of the comparative specimens were cited from Weidenreich (1937), Tobias and von Koenigswald (1964), Jacob (1973), Brown et al. (1985), Tobias (1991), Wood (1991), Grine and Franzen (1994), Bermúdez de Castro et al. (1999), Martínón-Torres et al., 2008, Martínón-Torres et al., 2012, Martínón-Torres et al., 2019, Arif et al. (2002), Zaim et al. (2011), and Xing et al., 2014, Xing et al., 2016. Refer to SOM Table S1 for the sources of crown size of the comparative specimens.

<sup>a</sup> The interproximal wear facet was taken into account and restored following the profile of the crown contour.

<sup>b</sup> PA 105-4 = RM<sup>2</sup> and RM<sup>3</sup>; PA 105-6 = LM<sup>2</sup>.

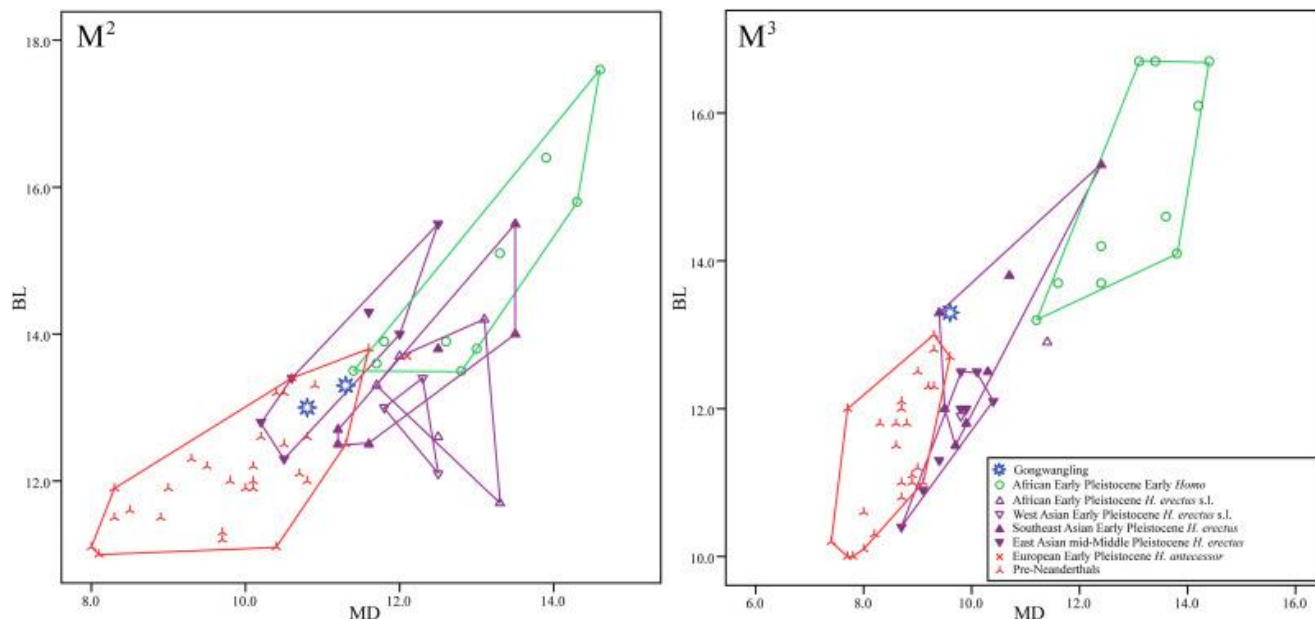


Figure 5. Bivariate plots of the mesiodistal (MD) vs. buccolingual (BL) diameters of the Gongwangling  $RM^2$  and  $LM^2$  (left panel) and  $RM^3$  (right panel) and comparative fossil hominins. The Gongwangling  $RM^2$  and  $LM^2$  fall within the range of variation for East Asian mid-Middle Pleistocene *Homo erectus* and pre-Neanderthals, while its  $RM^3$  falls within the range of variation for Southeast Asian Early Pleistocene *Homo erectus*.

R = right; L = left.

The MD diameter of the Gongwangling  $RM^3$  falls within the lower end of the range of variation for Southeast Asian Early Pleistocene *H. erectus* and within the range of East Asian mid-Middle Pleistocene *H. erectus* (Table 2). It is smaller than those of African early Pleistocene *Homo*, African Early Pleistocene *H. erectus* s.l., and West Asian Early Pleistocene *H. erectus* s.l. The BL diameter of the Gongwangling  $RM^3$  falls within the range of variation for Southeast Asian Early Pleistocene *H. erectus*, but is larger than African Early Pleistocene *H. erectus* s.l., West Asian Early Pleistocene *H. erectus* s.l., and East Asian mid-Middle Pleistocene *H. erectus* (Table 2). It falls within the lower end of the African early Pleistocene *Homo* range of variation. The bivariate plot shows that the Gongwangling  $M^3$  falls within the range of variation for Southeast Asian Early Pleistocene *H. erectus* (Fig. 5).

#### 3.4. Enamel thickness of the upper third molar

Two-dimensional measurements of the enamel cap area of the Gongwangling  $RM^3$  provided values of 26.56 and 28.91 mm<sup>2</sup> before and after restoration of the occlusal wear, respectively (see SOM Fig. S2). The coronal dentine area measures 48.06 mm<sup>2</sup>, and the 2D AET and RET were calculated for the corrected enamel area, providing values of 1.38 mm and 19.87, respectively (while the 2D AET and 2D RET computed with uncorrected values of the enamel area give values of 1.27 mm and 18.25, respectively). Three-dimensional enamel volume and coronal dentine volume are 326.92 and 370.62 mm<sup>3</sup>, respectively, and 3D AET and RET are calculated as 1.34 mm and 18.63, respectively.

The corrected 2D AET of the Gongwangling  $RM^3$  is larger than the value for Steinheim and smaller than the value for Thomas Quarry. It falls within the range of pre-Neanderthals and modern humans, just slightly exceeding the Neanderthal range (by 0.03 mm; Table 3; SOM

Fig. S3). The corrected 2D RET of the Gongwangling RM<sup>3</sup> is smaller than Steinheim and Thomas Quarry and falls just below the range of pre-Neanderthals. It falls above the range of Neanderthals and within the range of variation of modern humans.

Table 3. Two dimensional (2D) and three dimensional (3D) average (AET) and relative (RET) enamel thickness variables for the Gongwangling RM<sup>3</sup> and extinct and extant specimens/populations included in this study.<sup>a</sup>

Sample	<i>n</i>	Descriptive statistics	2D AET (mm)	2D RET	Source
Gongwangling	1		1.38 (1.27) <sup>a</sup>	19.87 (18.25) <sup>a</sup>	
North African <i>Homo</i> (Thomas Quarry)	1		1.56	22.96	Smith et al. (2012)
European Middle Pleistocene <i>Homo</i> (Steinheim)	1		1.25	21.59	Smith et al. (2012)
Pre-Neanderthals (Atapuerca Sima de los Huesos)	14	Mean	1.3	23.84	Martín-Francés et al. (2020)
		SD	0.13	2.07	
		Range	1.04–1.46	19.88–27.56	
Neanderthals	6	Mean	1.1	16.45	Olejniczak et al. (2008) Bayle et al. (2017)
		SD	0.19	1.94	
		Range	0.79–1.35	13.82–18.49	
Modern humans	11	Mean	1.30	22.38	Martin (1983); Martín-Francés et al. (2020)
		SD	0.20	4.10	
		Range	1.01–1.64	16.63–28.99	
Sample	<i>n</i>		3D AET (mm)	3D RET	
Gongwangling	1		1.34	18.63	
<i>Homo erectus</i> (NG0802.1 from Sangiran)	1		1.45	27.64	Zanolli (2015)
Pre-Neanderthals (Atapuerca Sima de los Huesos)	14	Mean	1.36	25.39	Martín-Francés et al. (2020)
		SD	0.11	2.06	

Sample	<i>n</i>	Descriptive statistics	2D AET (mm)	2D RET	Source
Neanderthals	9	Range	1.18– 1.50	21.24– 30.02	Olejniczak et al. (2008); Bayle et al. (2013)
		Mean	1.03	15.62	
		SD	0.14	2.05	
Modern humans	22	Range	0.75– 1.18	11.61– 18.43	Olejniczak et al. (2008); Martín-Francés et al. (2020)
		Mean	1.44	26.10	
		SD	0.24	5.14	
		Range	0.91– 1.94	14.54– 34.10	

Abbreviations: AET = average enamel thickness; RET = relative enamel thickness.

<sup>a</sup> Values corrected for occlusal wear are shown first, followed by the uncorrected values in parentheses.

The 3D AET of Gongwangling is smaller than NG0802.1 (Sangiran *H. erectus*), falls within the range of pre-Neanderthals and modern humans, and above the range of Neanderthals. The 3D RET of the Gongwangling RM<sup>3</sup> is smaller than NG0802.1 (Sangiran *H. erectus*), falls below the range of pre-Neanderthals, and within the range of variation of modern humans. In sum, enamel thickness of the Gongwangling RM<sup>3</sup> can be included in the range of variation of modern humans but is relatively thicker than Neanderthals (both 2D and 3D) and relatively thinner than that of the comparative Early and Middle Pleistocene hominins included in this study.

### 3.5. Diffeomorphic surface matching of the enamel-dentine junction

Plots of the PCA are presented in SOM Figure S4. The results of the bgPCA based on the DSM analysis of the RM<sup>2</sup> EDJ show that bgPC1 and bgPC2 explain 64.7% and 34.9% of the total shape variation, respectively (Fig. 6). The specimens with positive bgPC1 scores tend to have a symmetrical and trapezoidal crown outline with the mesial half being buccolingually wider than the distal one. The crista obliqua is low, and the hypocone is reduced in size. The teeth with bgPC1 negative scores display a skewed crown with a protruding paracone and an enlarged hypocone. The dentine horns are high, especially for the protocone and hypocone. The specimens with positive bgPC2 scores tend to have a trapezoidal crown outline with the mesial part being buccolingually wider than the distal one. The crown shape of specimens with negative bgPC2 scores is buccolingually elongated and oval-like. Pre-Neanderthals and Neanderthals are distributed along the negative end of bgPC1 (except for one Neanderthal specimen, Krapina D99), while most modern humans are distributed along the positive end of bgPC1 and negative space of bgPC2. All the comparative Southeast Asian Early Pleistocene *H. erectus* and East Asian mid-Middle Pleistocene specimens are distributed along the positive end of bgPC1 and bgPC2, with those from the Early Pleistocene distributed more toward the positive-value end. The Gongwangling RM<sup>2</sup> does not plot within the range of *H. erectus* or Neanderthals but falls

closest to and just outside the modern human range. The typicality probabilities are below 0.05, suggesting that Gongwangling RM<sup>2</sup> cannot be confidently attributed to any of the comparative groups (Table 4). The results of the CVA reveal a clear separation among *H. erectus* s.l., pre-Neanderthals and Neanderthals, and modern humans (Fig. 7), with Early and Middle Pleistocene *H. erectus* groups largely overlapping. The Gongwangling RM<sup>2</sup> plots outside of the range of the three comparative groups, but closer to *H. erectus*. The posterior probability classifies the Gongwangling M<sup>2</sup> as *H. erectus* (100% probability; Table 4).

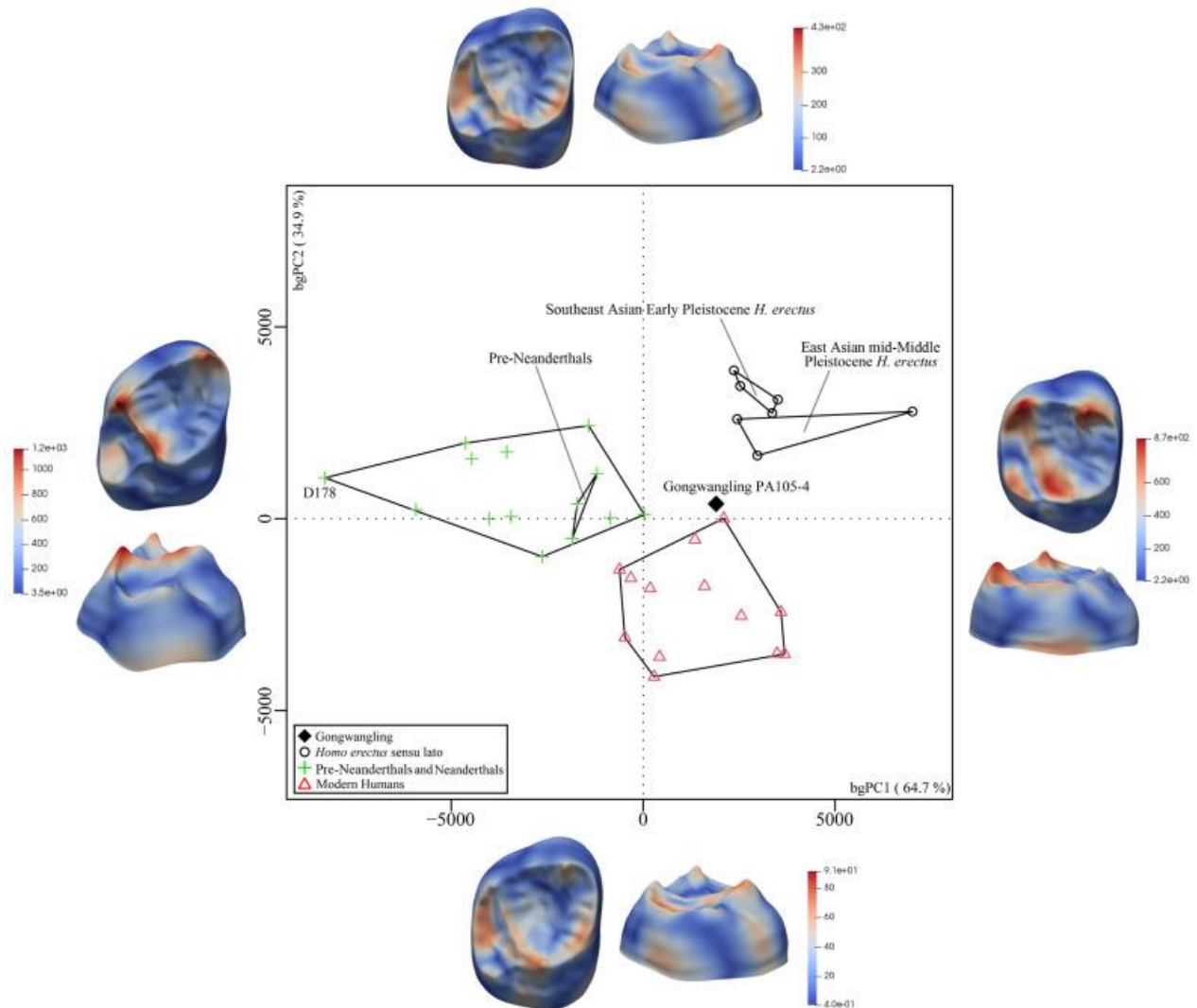


Figure 6. Bivariate plot of between-group principal component 2 (bgPC2) against bgPC1 based on the diffeomorphic surface matching analysis of the enamel-dentine junction of the Gongwangling RM<sup>2</sup> compared with *Homo erectus* s.l., pre-Neanderthals and Neanderthals, and modern humans. The magnitude of displacements between global mean shape to each extreme conformation was rendered as colormaps from dark blue (lowest values) to red (highest values) onto the enamel-dentine junction surfaces. The scale bar is in  $\mu\text{m}$ . R = right.

Table 4. Typicality probabilities of the between-group principal component analyses (bgPCA) and posterior probabilities of the canonical variate analyses (CVA) computed for the Gongwangling RM<sup>2</sup> and RM<sup>3</sup>.<sup>a</sup>

Tooth	<i>H. erectus</i> s.l.		Pre-Neanderthals and Neanderthals		Modern humans	
	bgPCA	CVA	bgPCA	CVA	bgPCA	CVA
RM <sup>2</sup>	0.03	100%	0.03	0%	0.03	0%
RM <sup>3</sup>	0.10	100%	0.00	0%	0.00	0%

Abbreviation: R = right.

<sup>a</sup> For the typicality probabilities of bgPCA, if the highest value is below 0.05, it suggests that the tooth can be considered as an outlier with respect of the groups analyzed here.

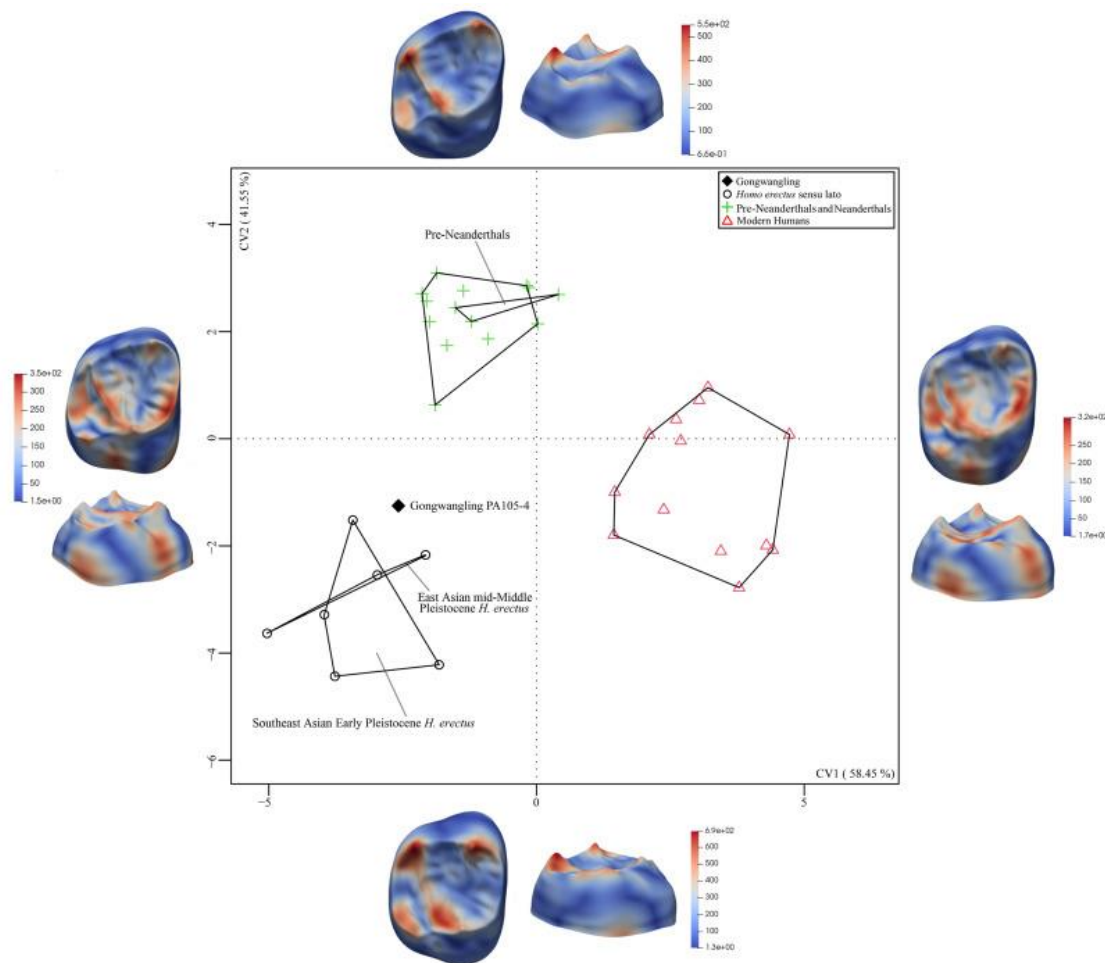


Figure 7. Bivariate plot of the canonical variate 2 (CV2) against CV1 based on the diffeomorphic surface matching analysis of the enamel-dentine junction of the Gongwangling RM<sup>2</sup> compared with *Homo erectus* s.l., pre-Neanderthals and Neanderthals, and modern humans. The magnitude of displacements between global mean shape to each extreme conformation was rendered as colormaps from dark blue (lowest values) to red (highest values) onto the enamel-dentine junction surfaces. The scale bar is in  $\mu\text{m}$ . R = right.

Results of the PCA are presented in SOM Figure S4. The results of the bgPCA computed on the DSM of the M<sup>3</sup> EDJ indicate that bgPC1 and bgPC2 explain 74.08% and 25.48% of the total shape variation, respectively (Fig. 8). Specimens with positive bgPC1 scores tend to have low crowns with short and internally displaced dentine horns of the paracone, protocone, and metacone. The hypocone is well developed, with an easily visible dentine horn, and the crista obliqua is not elevated. By contrast, specimens with negative bgPC1 scores tend to have high crowns with high and peripherally located dentine horns, and the hypocone tends to be markedly reduced and low. Compared to specimens with positive bgPC2 scores, those at the negative end tend to have asymmetrical crowns with a bulging paracone and a lingually placed metacone dentine horn. The dentine horns of the protocone and metacone occupy a relatively more distal position. Most pre-Neanderthals and Neanderthals are distributed along the negative end of bgPC1 and positive end of bgPC2. Most modern humans are plotted along the negative scores of bgPC2. All African Early Pleistocene, Southeast Asia Early Pleistocene, and East Asian mid-Middle Pleistocene, *H. erectus* s.l. specimens are distributed along the positive end of bgPC1, with Early and Middle Pleistocene teeth overlapping. The Gongwangling RM<sup>3</sup> falls closest to *H. erectus* s.l., and the typicality probabilities show that it is compatible with the range of variation of *H. erectus* s.l. (Table 4). The CVA also shows a marked separation between *H. erectus* s.l., pre-Neanderthals, Neanderthals, and modern humans (Fig. 9). Pre-Neanderthals and Neanderthals largely overlap with each other as do Early and Middle Pleistocene *H. erectus* s.l. The Gongwangling RM<sup>3</sup> falls inside the range of *H. erectus* s.l. and is classified as *H. erectus* s.l. based on the posterior probability (100%; Table 4).

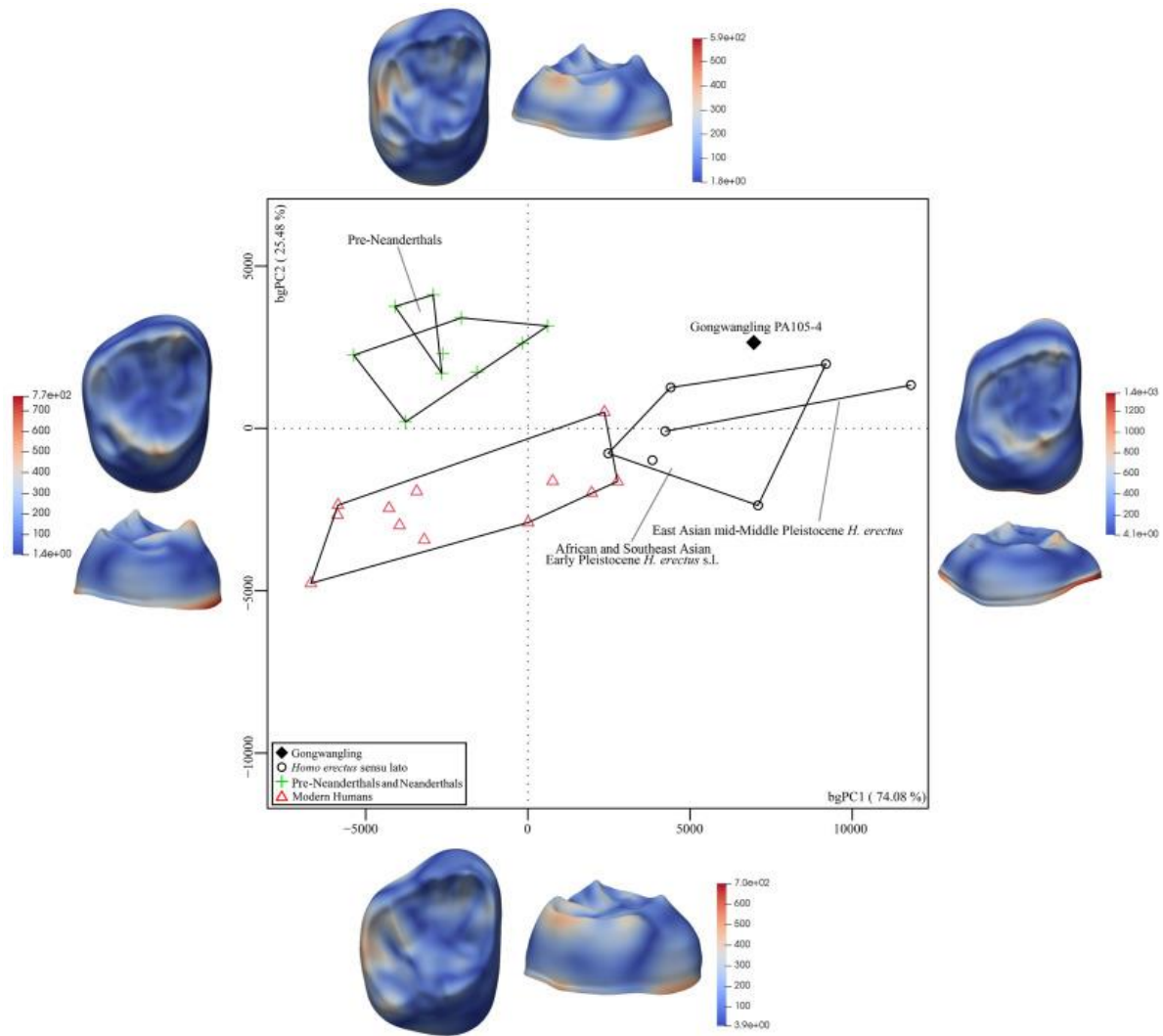


Figure 8. Bivariate plot of the between-group principal component 2 (bgPC2) against bgPC1 based on the diffeomorphic surface matching analysis of the enamel-dentine junction of the Gongwangling RM<sup>3</sup> compared with *Homo erectus* s.l., pre-Neanderthals and Neanderthals, and modern humans. The magnitude of displacements between global mean shape to each extreme conformation was rendered as colormaps from dark blue (lowest values) to red (highest values) onto the enamel-dentine junction surfaces. The scale bar is in  $\mu\text{m}$ . R = right.

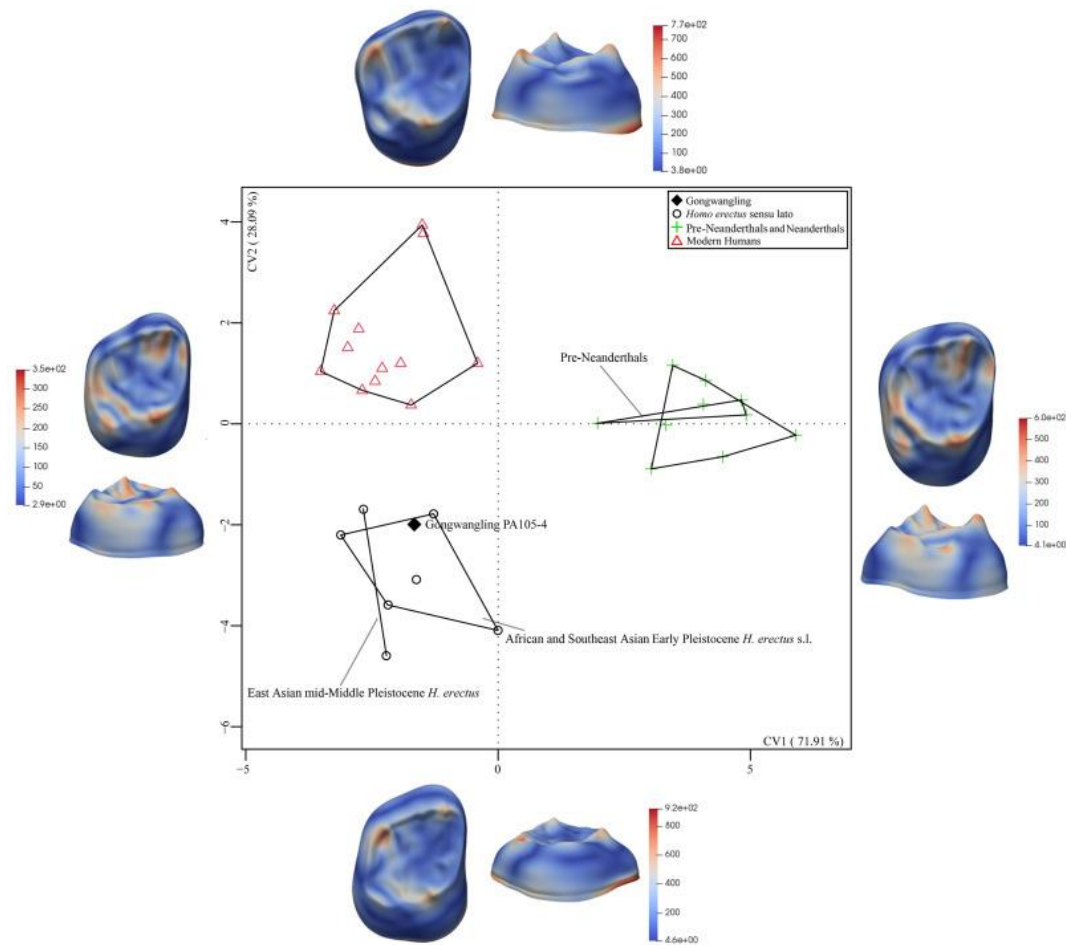


Figure 9. Bivariate plot of the canonical variate 2 (CV2) against CV1 based on the diffeomorphic surface matching analysis of the enamel-dentine junction of the Gongwangling RM<sup>3</sup> compared with *Homo erectus* s.l., pre-Neanderthals and Neanderthals, and modern humans. The magnitude of displacements between global mean shape to each extreme conformation was rendered as colormaps from dark blue (lowest values) to red (highest values) onto the enamel-dentine junction surfaces. The scale bar is in  $\mu\text{m}$ . R = right.

#### 4. Discussion and conclusions

The Gongwangling individual is one of the earliest members of *H. erectus* s.l. ever recovered in East Asia (An and Ho, 1989; Zhu et al., 2015). Due to severe taphonomic distortion (i.e., cranial bones are broken and heavily crushed), the Gongwangling cranium cannot be used alone to infer any clear evolutionary relationship with other members of the species. Fortunately, six maxillary teeth from the same individual were preserved, three of them with relatively complete crowns, which allowed us to assess affinities of the Gongwangling individual with *H. erectus* s.l. from Africa, West Asia, Southeast Asia, and East Asia.

In terms of crown size, the M<sup>2</sup>s of Gongwangling are compatible with the variation of East Asian Middle Pleistocene *H. erectus* (Fig. 5; Table 3). Compared to other Early Pleistocene *H. erectus* s.l. specimens (i.e., African, Dmanisi, and Sangiran material), the Gongwangling M<sup>2</sup>s have smaller crowns and fall outside their ranges of variation, especially in the MD diameter. However, RM<sup>3</sup> crown size falls within the range of variation for Southeast

Asian Early Pleistocene specimens. In both MD and BL diameters, the Gongwangling M<sup>2</sup>s are smaller than those of the ~1.5 Ma *H. erectus* specimen Bpg 2001.04 from the Sangiran site of Bapang (Zaim et al., 2011). The Gongwangling RM<sup>3</sup> has a larger crown than East Asian Middle Pleistocene *H. erectus*, especially in its BL diameter.

The medium-sized hypocone of the M<sup>2</sup>s and small hypocone of the RM<sup>3</sup> place the Gongwangling individual at the lower end of the variation for Early Pleistocene *H. erectus* s.l. and Middle Pleistocene *H. erectus* s.l. The crown shape of Gongwangling M<sup>2</sup>s is different from that of *H. antecessor*, with the latter being skewed and with a bulging hypocone (Bermúdez de Castro et al., 2021). Likely, the *H. antecessor* M<sup>1</sup> also has a skewed crown outline and an enlarged hypocone that protrudes in both distal and lingual directions. This distinct crown shape is not observed in Meipu, another Early Pleistocene hominin from East Asia (Gómez-Robles et al., 2007; Martín-Torres et al., 2019; Bermúdez de Castro et al., 2021; Xing et al., 2021). In addition to the skewed crown outline of M<sup>1</sup> and M<sup>2</sup>, other dental features of *H. antecessor* (e.g., continuous middle trigonid crest of lower molars) aligned with the Neanderthal-lineage dental pattern (Bailey, 2002; Martín-Torres et al., 2007). Comparatively, these typical traits in *H. antecessor*, as well as in pre-Neanderthals and Neanderthals (Bailey, 2002; Martín-Torres et al., 2007), are not present in East Asian Early Pleistocene hominins including Meipu (Xing et al., 2021) and Gongwangling, and East Asian Middle Pleistocene *H. erectus* from Zhoukoudian, Hexian, and Yiyuan (Xing et al., 2014, 2016; Bermúdez de Castro et al., 2021). These morphological differences likely reflect two distinct evolutionary paths for the European (*H. antecessor*) and the Asian (*H. erectus*) populations as early as the Early Pleistocene (Bermúdez de Castro et al., 2021).

Results of enamel thickness show that the RM<sup>3</sup> of PA105 has thick enamel despite the wear. Occlusal wear may influence the measurement of enamel thickness and affect the comparison between Gongwangling and other specimens included in the present study, especially for the 3D estimates. For this reason, the 2D estimates have been corrected for wear and more closely approximate the original condition of the specimen. Since the comparative samples generally include either unworn teeth or values corrected for wear, our analysis suggests that the Gongwangling specimen has thick enamel like that of most *Homo* species (besides Neanderthals and a few exceptions), even if less thick than the late Early to early-Middle Pleistocene *H. erectus* specimen NG0802.1 from Sangiran (Zanolli, 2015).

The unique dendrite-like EDJ surface with excessive ridges and grooves identified in Hexian and Yiyuan (Xing et al., 2014, 2016) is not observed in Gongwangling. This finding is in accordance with previous studies of the Gongwangling cranium that revealed more primitive features than in Zhoukoudian *H. erectus* (Woo, 1966a). In terms of EDJ shape, the M<sup>2</sup>s and M<sup>3</sup>s of Early and Middle Pleistocene *H. erectus* s.l. are similar and overlap in the bgPCA and CVA analyses. The Gongwangling individual shows a global affinity with *H. erectus* s.l. in these features although it lacks the derived traits typically found in later Asian Middle Pleistocene *H. erectus*. In the bgPCA analysis of the RM<sup>2</sup>, the Gongwangling specimen appears to be more similar to modern humans than to *H. erectus* s.l. and particularly along bgPC2. This is likely due to the fact that differences captured along this axis are subtle and PA105 shows a morphology that is slightly different from the limited comparative sample available for *H. erectus* s.l. It is also relevant that the Gongwangling RM<sup>2</sup> unambiguously falls with *H. erectus* s.l. in the CVA (that is based on the PC scores, and not on the shape data as it is the case for the bgPCA). Taking into consideration both the bgPCA and the CVA, the Gongwangling molars seem to be closer to Middle Pleistocene *H. erectus* than to other Early Pleistocene members. This may imply that the shape of

the crown at the dentine level in Middle Pleistocene *H. erectus* was already present in the Early Pleistocene *H. erectus*.

The radicals of the molar roots are completely separated and highly divergent (especially in the M<sup>3</sup>), a feature generally found in australopithecines, Early Pleistocene *H. erectus* s.l. (e.g., Sangiran 17; Kaifu, 2006), and African early *Homo*, but absent in East Asian Middle Pleistocene *H. erectus* from Zhoukoudian, where the three-radical root is typically fused (Weidenreich, 1937; Moggi-Cecchi et al., 2006; Zanolli et al., 2018a). However, Gongwangling roots are more robust than those from Dmanisi and Meipu, approaching the East Asian Middle Pleistocene *H. erectus* condition, with column-like shape radicals like in the Hexian teeth (even if not as markedly as in the latter).

The six teeth of the Gongwangling individual exhibit dental nonmetric traits and crown diameters that are comparable to Early Pleistocene members of *H. erectus* s.l. and differ from Middle Pleistocene members of this species. However, geometric morphometric analyses of the EDJ of the molars suggest that an Asian pattern was already prefigured in the Early Pleistocene. The limited number of well-preserved hominin fossils with clear provenance from the East Asian Early Pleistocene (Hu, 1973; Li and Etlér, 1992) hampers our understanding of their phylogenetic relationships with other members of the genus *Homo* from approximately the same chronological age or territory. The re-evaluation of Early Pleistocene hominin remains from Gongwangling, Meipu (Xing et al., 2021) and other material with relatively secure and reliable geological information will help to better inform the morphological variability and evolutionary trajectories of *H. erectus* in Asia. The recent morphometric analyses of the Meipu teeth (Xing et al., 2021), dated to 0.99–0.78 Ma, showed that the specimens are intermediate between African/Dmanisi Early Pleistocene hominins and East Asian Middle Pleistocene *H. erectus*. Early Pleistocene hominins from Quyuan River Mouth from approximately the same chronological age as Meipu surprisingly exhibit a peg-like M<sup>3</sup> (Li and Etlér, 1992) while keeping a primitive P<sup>4</sup> crown outline with a mesiodistally longer lingual cusp than the buccal one (Xing et al., 2021). These limited samples from Gongwangling, Meipu, and Quyuan River Mouth display some variability for East Asian Early Pleistocene *H. erectus*, and dental characteristics that are more primitive than those of East Asian Middle Pleistocene *H. erectus*. The Early to Middle Pleistocene variability in dental traits is compatible with a potential temporal variation in East Asian continental *H. erectus*. The analysis of dental structure of more specimens of the *H. erectus* s.l. hypodigm, like those from Dmanisi and eastern Africa, would be required to further understand the chrono-geographic variations of this taxon and evolutionary trajectories during the Early Pleistocene.

### **Declaration of competing interest**

The authors declare no conflict of interest.

### **Acknowledgments**

As one part of this special issue, the work of Gongwangling teeth is dedicated to Pan Lei, a young and talented scholar as well as our beloved friend. Pan Lei reinitiated the study of Gongwangling teeth, and we are honored to complete her work and publish it. J. L. Arsuaga, E. Carbonell, R. Clarke, J. Svoboda, I. Tattersall, K. Mowbray, G. Sawyer, J. de Vos, H. de Lumley, M.-A. de Lumley, A. Vialet, P. Tassy, Y. Kaifu, and M. Zhou kindly provided opportunities to observe or take photos of the comparative specimens used in this study and helped us in a variety of other ways. J. Dumoncel kindly gave us instructions for the DSM analyses. Y.M. Hou helped us with scanning the Gongwangling fossil and other specimens. J. Zuo virtually reconstructed the

teeth of Gongwangling. The authors want to express their gratitude to all these colleagues. Many thanks to the four anonymous reviewers who spent time on this work and who greatly improved the paper with valuable suggestions. This work was supported by the Strategic Priority Research Program of the Chinese Academy of Sciences (No. XDA19050102; No. XDB26000000), the National Natural Science Foundation of China (41702026, 41872030), French Centre National de la Recherche Scientifique (CNRS), Ministerio de Economía y Competitividad (PGC2018-093925-B-C31), State Key Laboratory of Palaeobiology and Stratigraphy (Nanjing Institute of Geology and Palaeontology, CAS; No. 173119), British Academy (International Partnership and Mobility Scheme PM160019), and the Leakey Foundation through the personal support of D. Crook to one of the authors (M.M.-T).

## References

- Aigner, J.S., Laughlin, W.S., 1973. The dating of Lantian man and his significance for analyzing trends in human evolution. *Am. J. Phys. Anthropol.* 39, 97–109.
- An, Z.S., Ho, C.K., 1989. New magnetostratigraphic dates of Lantian *Homo erectus*. *Quat. Res.* 32, 213–221.
- Antón, S.C., 2003. Natural history of *Homo erectus*. *Am. J. Phys. Anthropol.* 122, 126–170.
- Arif, J., Kaifu, Y., Baba, H., Suparka, M.E., Zaim, Y., Setoguchi, T., 2002. Preliminary observation of a new cranium of *Homo erectus* (Tjg-1993.05) from Sangiran, Central Jawa. *Anthropol. Sci.* 110, 165–177.
- Bailey, S.E., 2002. A closer look at Neanderthal postcanine dental morphology: The mandibular dentition. *Anat. Rec.* 269, 148–156.
- Bayle, P., Mazurier, A., Macchiarelli, R., 2013. The permanent “virtual dentition”. In: Rougier, H., Semal, P. (Eds.), *Spy Cave. 125 Years of Multidisciplinary Research at the Betche aux Rotches (Jemeppe-sur-Sambre, Province of Namur, Belgium)*, vol. 2. *Anthropologica et Praehistorica* 124/2013, Royal Belgian Institute of Natural Sciences, Royal Belgian Society of Anthropology and Praehistory & NESPOS Society, Brussels.
- Bayle, P., Le Luyer, M., Robson Brown, K. A., 2017. The Palomas dental remains: Enamel thickness and tissues proportions. In: Trinkaus, E., Walker, M. J. (Eds.), *The people of Palomas: Neandertals From the Sima de las Palomas del Cabezo Gordo, Southeastern Spain*. Texas A&M University Anthropology Series, College Station, Texas, pp. 115–137.
- Beaudet, A., Dumoncel, J., Thackeray, F., Bruxelles, L., Duployer, B., Tenailleau, C., Bam, L., Hoffman, J., de Beer, F., Braga, J., 2016. Upper third molar internal structural organization and semicircular canal morphology in Plio-Pleistocene South African cercopithecoids. *J. Hum. Evol.* 95, 104–120.
- Benazzi, S., Kullmer, O., Grosse, I.R., Weber, G.W., 2011. Using occlusal wear information and finite element analysis to investigate stress distributions in human molars. *J. Anat.* 219, 259–272.
- Benazzi, S., Panetta, D., Fornai, C., Toussaint, M., Gruppioni, G., Hublin, J.-J., 2014. Technical Note: Guidelines for the digital computation of 2D and 3D enamel thickness in hominoid teeth. *Am. J. Phys. Anthropol.* 153, 305–313.
- Bermúdez de Castro, J.M., Rosas, A., Nicolás, M.E., 1999. Dental remains from Atapuerca-TD6 (Gran Dolina site, Burgos, Spain). *J. Hum. Evol.* 37, 523–566.
- Bermúdez de Castro, J.M., Xing, S., Liu, W., García-Campos, C., Martín-Francés, L., Martínez de Pinillos, M., Modesto-Mata, M., Martín-Torres, M., 2021. Comparative dental study between *Homo antecessor* and Chinese *Homo erectus*: Nonmetric features and geometric morphometrics. *J. Hum. Evol.* 161, 103087.

- Braga, J., Zimmer, V., Dumoncel, J., Samir, C., de Beer, F., Zanolli, C., Pinto, D., Rohlf, F.J., Grine, F.E., 2019. Efficacy of diffeomorphic surface matching and 3D geometric morphometrics for taxonomic discrimination of Early Pleistocene hominin mandibular molars. *J. Hum. Evol.* 130, 21–35.
- Brown, F., Harris, J., Leakey, R., Walker, A., 1985. Early *Homo erectus* skeleton from west Lake Turkana, Kenya. *Nature* 316, 788-792.
- Cardini, A., Polly, P.D., 2020. Cross-validated between group PCA scatterplots: A solution to spurious group separation? *Evol. Biol.* 47, 85-95.
- Cheng, G.L., Li, S.L., Lin, J.L., 1978. A research on the ages of the strata of “Lantian Man”. *Collected Papers of Palaeoanthropology*. Science Press, Beijing, pp. 151-157 (in Chinese).
- Delson, E., Tattersall, I., Couvering, J., Brooks, A.S., 2000. *Encyclopedia of Human Evolution and Prehistory*. Garland Publishing, New York.
- Dray, S., Dufour, A.-B., 2007. The ade4 package: Implementing the duality diagram for ecologists. *J. Stat. Softw.* 22, 1–20.
- Dumoncel, J., Durrleman, S., Braga, J., Jessel, J.-P., Subsol, G., 2014a. Landmark-free 3D method for comparison of fossil hominins and hominids based on endocranium and EDJ shapes. *Am. J. Phys. Anthropol.* 153, suppl. 56, 110.
- Durrleman, S., Penneç, X., Trouvé, A., Ayache, N., Braga, J., 2012a. Comparison of the endocranial ontogenies between chimpanzees and bonobos via temporal regression and spatiotemporal registration. *J. Hum. Evol.* 62, 74–88.
- Durrleman, S., Prastawa, M., Korenberg, J.R., Joshi, S., Trouvé, A., Gerig, G., 2012b. Topology preserving atlas construction from shape data without correspondence using sparse parameters. In: Ayache, N., Delingette, H., Golland, P., Mori, K. (Eds.), *Proceedings of Medical Image Computing and Computer Assisted Intervention*. Nice, France, pp. 223–230
- Durrleman, S., Prastawa, M., Charon, N., Korenberg, J.R., Joshi, S., Gerig, G., Trouvé, A., 2014b. Morphometry of anatomical shape complexes with dense deformations and sparse parameters. *NeuroImage* 101, 35–49.
- Fajardo, R.J., Ryan, T., Kappelman, J., 2002. Assessing the accuracy of high-resolution X-ray computed tomography of primate trabecular bone by comparisons with histological sections. *Am. J. Phys. Anthropol.* 118, 1–10.
- Gómez-Robles, A., Martínón-Torres, M., De Castro, J.B., Margvelashvili, A., Bastir, M., Arsuaga, J.L., Pérez-Pérez, A., Estebananz, F., Martínez, L.M., 2007. A geometric morphometric analysis of hominin upper first molar shape. *J. Hum. Evol.* 53, 272–285.
- Grine, F., Franzen, J.L., 1994. Fossil hominid teeth from the Sangiran Dome (Java, Indonesia). *Cour. Forsch. Inst. Senckenb.* 171, 75–103.
- Hu, C., 1973. Ape-man teeth from Yuanmou, Yunnan. *Acta Geol. Sin.* 1, 65-71.
- Hughes, A.R., Tobias, P.V., 1977. A fossil skull probably of the genus *Homo* from Sterkfontein, Transvaal. *Nature* 265, 310–312.
- Jacob, T., 1973. Palaeoanthropological discoveries in Indonesia with special reference to the finds of the last two decades. *J. Hum. Evol.* 2, 473-485.
- Kaifu, Y., 2006. Advanced dental reduction in Javanese *Homo erectus*. *Anthropol. Sci.* 114, 35-43.
- Kono, R., 2004. Molar enamel thickness and distribution patterns in extant great apes and humans, new insights based on a 3-dimensional whole crown perspective. *Anthropol. Sci.* 112, 121–146.
- Li, T., Etler, D.A., 1992. New Middle Pleistocene hominid crania from Yunxian in China. *Nature* 357, 404-407.

- Liu, W., Martínón-Torres, M., Kaifu, Y., Wu, X., Kono, R., Chang, C.-H., Wei, P., Xing, S., Huang, W., Bermúdez de Castro, J.M., 2017. A mandible from the Middle Pleistocene Hexian site and its significance in relation to the variability of Asian *Homo erectus*. *Am. J. Phys. Anthropol.* 162, 715–731.
- Ma, X.H., Qian, F., Li, P., Ju, S.Q., 1978. Paleomagnetic dating of Lantian Man. *Vertebr. Palasiatica* 16, 238-243.
- Macchiarelli, R., Bayle, P., Bondioli, L., Mazurier, A., Zanolli, C., 2013. From outer to inner structural morphology in dental anthropology: Integration of the third dimension in the visualization and quantitative analysis of fossil remains. In: Scott, G.R., Irish, J. (Eds.), *Anthropological Perspectives on Tooth Morphology: Genetics, Evolution, Variation*. Cambridge University Press, Cambridge, pp. 250-277.
- Martin, L.B., 1983. The relationships of the later Miocene Hominoidea. Ph.D. Dissertation, University of London.
- Martín-Francés, L., Martínón-Torres, M., Martínez de Pinillos, M., García-Campos, C., Zanolli, C., Bayle, P., Modesto-Mata, M., Arsuaga, J.L., Bermúdez de Castro, J.M., 2020. Crown tissue proportions and enamel thickness distribution in the Middle Pleistocene hominin molars from Sima de los Huesos (SH) population (Atapuerca, Spain). *PLoS One* 15, e0233281.
- Martinón-Torres, M., De Castro, J.B., Gómez-Robles, A., Arsuaga, J.L., Carbonell, E., Lordkipanidze, D., Manzi, G., Margvelashvili, A., 2007. Dental evidence on the hominin dispersals during the Pleistocene. *Proc. Nat. Acad. Sci. USA* 104, 13279–13282.
- Martinón-Torres, M., Bermúdez de Castro, J.M., Gómez-Robles, A., Margvelashvili, A., Prado, L., Lordkipanidze, D., Vekua, A., 2008. Dental remains from Dmanisi (Republic of Georgia): morphological analysis and comparative study. *J. Hum. Evol.* 55, 249–273.
- Martinón-Torres, M., Bermúdez de Castro, J.M., Gómez-Robles, A., Prado-Simón, L., Arsuaga, J., 2012. Morphological description and comparison of the dental remains from Atapuerca-Sima de los Huesos site (Spain). *J. Hum. Evol.* 62, 7–58.
- Martinón-Torres, M., Bermúdez de Castro, J.M., de Pinillos, M.M., Modesto-Mata, M., Song, X., Martín-Francés, L., García-Campos, C., Wu, X., Liu, W., 2019. New permanent teeth from Gran Dolina-TD6 (Sierra de Atapuerca). The bearing of *Homo antecessor* on the evolutionary scenario of Early and Middle Pleistocene Europe. *J. Hum. Evol.* 127, 93–117.
- Mitteroecker, P., Bookstein, F., 2011. Linear discrimination, ordination, and the visualization of selection gradients in modern morphometrics. *Evol. Biol.* 38, 100–114.
- Moggi-Cecchi, J., Grine, F.E., Tobias, P.V., 2006. Early hominid dental remains from Members 4 and 5 of the Sterkfontein Formation (1966–1996 excavations): Catalogue, individual associations, morphological descriptions and initial metrical analysis. *J. Hum. Evol.* 50, 239–328.
- Molnar, S., 1971. Human tooth wear, tooth function and cultural variability. *Am. J. Phys. Anthropol.* 34, 175–189.
- NESPOS database, 2021. Neanderthal Studies Professional Online Service. <https://www.nespos.org>.
- Olejniczak, A.J., 2006. Micro-computed tomography of primate molars. Ph.D. Dissertation, Stony Brook University.
- Olejniczak, A., Smith, T.M., Skinner, M.M., Grine, F.E., Feeney, R.N.M., Thackeray, J.F., Hublin, J.-J., 2008. Three-dimensional molar enamel distribution and thickness in *Australopithecus* and *Paranthropus*. *Biol. Lett.* 4, 406–410.

- Pan, L., Zanolli, C., 2019. Comparative observations on the premolar root and pulp canal configurations of Middle Pleistocene *Homo* in China. *Am. J. Phys. Anthropol.* 168, 637-646.
- Pan, L., Dumoncel, J., de Beer, F., Hoffman, J., Thackeray, J.F., Duployer, B., Tenailleau, C., Braga, J., 2016. Further morphological evidence on South African earliest *Homo* lower postcanine dentition: Enamel thickness and enamel dentine junction. *J. Hum. Evol.* 96, 82–96.
- Pan, L., Thackeray, J.F., Dumoncel, J., Zanolli, C., Oettlé, A., De Beer, F., Hoffman, J., Duployer, B., Tenailleau, C., Braga, J., 2017. Intra-individual metameric variation expressed at the enamel-dentine junction of lower post-canine dentition of South African fossil hominins and modern humans. *Am. J. Phys. Anthropol.* 163, 806–815.
- Pan, L., Dumoncel, J., Mazurier, A., Zanolli, C., 2019. Structural analysis of premolar roots in Middle Pleistocene hominins from China. *J. Hum. Evol.* 136, 102669.
- Pan, L., Dumoncel, J., Mazurier, A., Zanolli, C., 2020. Hominin diversity in East Asia during the Middle Pleistocene: A premolar endostructural perspective. *J. Hum. Evol.* 148, 102888.
- R Core Team, 2018. R: A language and environment for statistical computing. R Foundation for Statistical Computing, Vienna.
- Saunders, S.R., Chan, A.H.W., Kahlon, B., Kluge, H.F., FitzGerald, C.M., 2007. Sexual dimorphism of the dental tissues in human permanent mandibular canines and third premolars. *Am. J. Phys. Anthropol.* 133, 735-740.
- Schäfer, T., 2021. freesurferformats: Read and Write 'FreeSurfer' Neuroimaging File Formats. R software package.
- Schneider, C.A., Rasband, W.S., Eliceiri, K.W., 2012. NIH Image to ImageJ: 25 years of image analysis. *Nat. methods* 9, 671–675.
- Scott, G.R., Turner, C.G., 1997. *Anthropology of Modern Human Teeth*. Cambridge University Press Cambridge.
- Shang, H., Trinkaus, E., Liu, W., Wu, X., Zhu, Q., 2008. Neurocranial abnormalities of the Gongwangling *Homo erectus* from Lantian, China. *J. Archaeol. Sci.* 35, 2589–2593.
- Skinner, M.M., Wood, B.A., Boesch, C., Olejniczak, A.J., Rosas, A., Smith, T.M., Hublin, J.-J., 2008a. Dental trait expression at the enamel-dentine junction of lower molars in extant and fossil hominoids. *J. Hum. Evol.* 54, 173–186.
- Skinner, M.M., Gunz, P., Wood, B.A., Hublin, J.-J., 2008b. Enamel-dentine junction (EDJ) morphology distinguishes the lower molars of *Australopithecus africanus* and *Paranthropus robustus*. *J. Hum. Evol.* 55, 979–988.
- Skinner, M.M., Alemseged, Z., Gaunitz, C., Hublin, J.-J., 2015. Enamel thickness trends in Plio-Pleistocene hominin mandibular molars. *J. Hum. Evol.* 85, 35–45.
- Smith, T.M., Olejniczak, A.J., Zermeno, J.P., Tafforeau, P., Skinner, M.M., Hoffmann, A., Radović, J., Toussaint, M., Kruszynski, R., Menter, C., Moggi-Cecchi, J., Glasmacher, U.A., Kullmer, O., Schrenk, F., Stringer, C., Hublin, J.-J., 2012. Variation in enamel thickness within the genus *Homo*. *J. Hum. Evol.* 62, 395–411.
- Spoor, F., Hublin, J.-J., Braun, M., Zonneveld, F., 2003. The bony labyrinth of Neanderthals. *J. Hum. Evol.* 44, 141–165.
- Tobias, P.V., 1991. *Olduvai Gorge (The Skulls, Endocasts and Teeth of *Homo habilis*)*. Cambridge University Press, Cambridge.

- Tobias, P.V., Koenigswald, G.H.R.V., 1964. A comparison between the Olduvai Hominines and those of Java and some implications for hominid phylogeny. *Nature* 204, 515–518.
- Tu, H., Shen, G., Granger, D., Yang, X., Lai, Z., 2017. Isochron  $^{26}\text{Al}/^{10}\text{Be}$  burial dating of the Lantian hominin site at Gongwangling in northwestern China. *Quat. Geochronol.* 41, 174–179.
- Turner, C.G., Nichol, C.R., Scott, G.R., 1991. Scoring procedures for key morphological traits of the permanent dentition: the Arizona State University dental anthropology system, In: Kelley, M.A., Larsen, C.S. (Eds.), *Advances in Dental Anthropology*. Wiley-Liss, New York, pp. 31–31.
- Vialet, A., Guipert, G., Jianing, H., Xiaobo, F., Zune, L., Youping, W., Tianyuan, L., de Lumley, M.-A., de Lumley, H., 2010. *Homo erectus* from the Yunxian and Nankin Chinese sites: Anthropological insights using 3D virtual imaging techniques. *C. R. Palevol* 9, 331–339.
- Warnes, G.R., Bolker, B., Lumley, T., 2020. gtools: Various R Programming Tools. R software package.
- Weidenreich, F., 1937. The dentition of *Sinanthropus pekinensis*: A comparative odontography of the hominids. *Palaeontol. Sin. Series D I*, 1–180.
- Woo, J.-K., 1964. The new hominin tooth found in Lantian of Shaanxi (in Chinese). *Chin. Sci. Bull.* 10, 940–941.
- Woo, J.-K., 1965. Preliminary report on a skull of *Sinanthropus lantianensis* of Lantian, Shensi. *Sci. Sinica* 14, 1032–1036.
- Woo, J.-K., 1966a. The skull of Lantian man. *Curr. Anthropol.* 7, 83–86.
- Woo, J.-K., 1966b. The hominid skull of Lantian, Shensi (in Chinese with English abstract). *Vertebr. Palasiatica* 10, 1–16.
- Wood, B., 1991. Koobi Fora Research Project: Hominid Cranial Remains. Oxford University Press, USA.
- Wu, X., Zhang, Y., 2016. The temporal bony labyrinthine morphology of Lantian *Homo erectus* from Gongwangling, Shaanxi province. *Acta Anthropol. Sini* 2016, 35, 14–23.
- Xing, S., Martín-Torres, M., Bermúdez de Castro, J.M., Zhang, Y., Fan, X., Zheng, L., Huang, W., Liu, W., 2014. Middle Pleistocene hominin teeth from Longtan Cave, Hexian, China. *PLoS One* 9, e114265.
- Xing, S., Martín-Torres, M., Bermúdez de Castro, J.M., Wu, X., Liu, W., 2015. Hominin teeth from the early Late Pleistocene site of Xujiayao, Northern China. *Am. J. Phys. Anthropol.* 156, 224–240.
- Xing, S., Sun, C., Martín-Torres, M., Bermúdez de Castro, J.M., Han, F., Zhang, Y., Liu, W., 2016. Hominin teeth from the Middle Pleistocene site of Yiyuan, Eastern China. *J. Hum. Evol.* 95, 33–54.
- Xing, S., Martín-Torres, M., Bermúdez de Castro, J.M., 2018. The fossil teeth of the Peking Man. *Sci. Rep.* 8, 1–11.
- Xing, S., Martín-Torres, M., Deng, C., Shao, Q., Wang, Y., Luo, Y., Zhou, X., Pan, L., Ge, J., Bermúdez de Castro, J.M., Liu, W., 2021. Early Pleistocene hominin teeth from Meipu, southern China. *J. Hum. Evol.* 151, 102924.
- Zaim, Y., Ciochon, R.L., Polanski, J.M., Grine, F.E., Bettis, E.A., Rizal, Y., Franciscus, R.G., Larick, R.R., Heizler, M., Eaves, K.L., 2011. New 1.5 million-year-old *Homo erectus* maxilla from Sangiran (Central Java, Indonesia). *J. Hum. Evol.* 61, 363–376.
- Zanolli, C., 2015. Molar crown inner structural organization in Javanese *Homo erectus*. *Am. J. Phys. Anthropol.* 156, 148–157.

- Zanolli, C., Pan, L., Dumoncel, J., Kullmer, O., Kúndrát, M., Liu, W., Macchiarelli, R., Mancini, L., Schrenk, F., Tuniz, C., 2018a. Inner tooth morphology of *Homo erectus* from Zhoukoudian. New evidence from an old collection housed at Uppsala University, Sweden. *J. Hum. Evol.* 116, 1–13.
- Zanolli, C., Martínón-Torres, M., Bernardini, F., Boschian, G., Coppa, A., Dreossi, D., Mancini, L., Martínez de Pinillos, M., Martín-Francés, L., Bermúdez de Castro, J.M., Tozzi, C., Tuniz, C., Macchiarelli, R., 2018b. The Middle Pleistocene (MIS 12) human dental remains from Fontana Ranuccio (Latium) and Visogliano (Friuli-Venezia Giulia), Italy. A comparative high resolution endostructural assessment. *PLoS One* 13, e0189773.
- Zanolli, C., Kullmer, O., Kelley, J., Bacon, A.-M., Demeter, F., Dumoncel, J., Fiorenza, L., Grine, F.E., Hublin, J.-J., Tuan, N., Nguyen Thi, M.H., Pan, L., Schillinger, B., Schrenk, F., Skinner, M.M., Xueping, J., Macchiarelli, R., 2019. Evidence for increased hominid diversity in the Early-Middle Pleistocene of Java, Indonesia. *Nat. Ecol. Evol.* 3, 755-764.
- Zanolli, C., Kaifu, Y., Xing, S., Mijares, A.S., Kullmer, O., Schrenk, F., Corny, J., Dizon, E., Robles, E., Détroit, F., 2022. Further analyses of the structural organization of *Homo luzonensis* teeth: Evolutionary implications. *J. Hum. Evol.* 163, 103124.
- Zhu, R., Potts, R., Xie, F., Hoffman, K.A., Deng, C.L., Shi, C., Pan, Y.X., Wang, H.Q., Shi, R.P., Wang, Y., 2004. New evidence on the earliest human presence at high northern latitudes in northeast Asia. *Nature* 431, 559–562.
- Zhu, Z.Y., Dennell, R., Huang, W.W., Wu, Y., Rao, Z.G., Qiu, S.F., Xie J.B., Liu, W., Fu, S.Q., Han, J.W., Zhou, H.Y., Ou Yang, T.P., Li, H.M., 2015. New dating of the *Homo erectus* cranium from Lantian (Gongwangling), China. *J. Hum. Evol.*, 78, 144-157.